

AD-A164 308

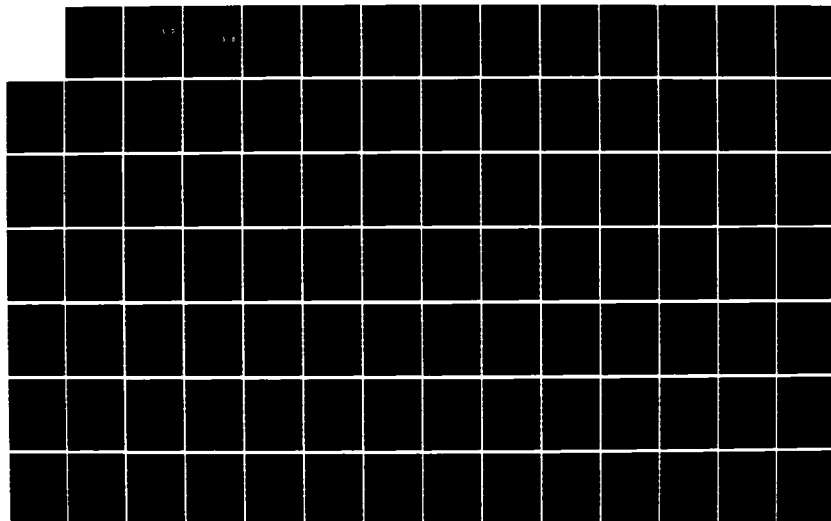
DETECTION OF ATMOSPHERIC CARBON DIOXIDE FROM A
SHUTTLE-BORNE LIDAR(U) AIR FORCE INST OF TECH
WRIGHT-PATTERSON AFB OH SCHOOL OF ENGINEERING R H WANK
DEC 82 AFIT/GE/PH/82D-25

1/2

UNCLASSIFIED

F/G 4/1

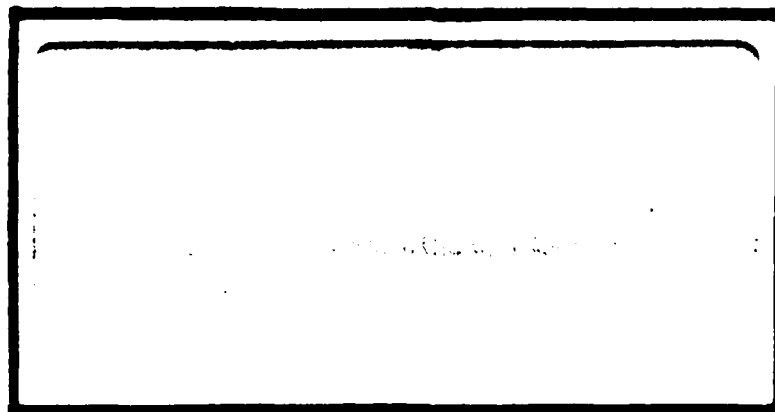
NL



AD-A164 308



DTIC
ELECTE
FEB 14 1986
S D



DTIC FILE COPY

DISTRIBUTION STATEMENT A

Approved for public release;
Distribution Unlimited

DEPARTMENT OF THE AIR FORCE

AIR UNIVERSITY

AIR FORCE INSTITUTE OF TECHNOLOGY

Wright-Patterson Air Force Base, Ohio

86 2 14 019

1

DTIC
ELECTE
FEB 14 1988
S D D

DETECTION OF ATMOSPHERIC
CARBON DIOXIDE FROM A
SHUTTLE-BORNE LIDAR

THESIS

AFIT/GEP/PH/82D-25

Robert H. Wank
Cpt. USA

DISTRIBUTION STATEMENT A
Approved for public release;
Distribution Unlimited

DETECTION OF ATMOSPHERIC
CARBON DIOXIDE FROM A
SHUTTLE-BORNE LIDAR

THESIS

Presented to the Faculty of the School of Engineering
of the Air Force Institute of Technology
Air University
in Partial Fulfillment of the
Requirements for the Degree of
Master of Science

by

Robert H. Wank, B.S.
Cpt. USA

Graduate Physics

December 1982

Accession For	
NTIS CRA&I	<input checked="checked" type="checkbox"/>
DTIC TAB	<input type="checkbox"/>
Unannounced	<input type="checkbox"/>
Justification	
By	
Distribution/	
Availability Codes	
Dist	Avail and/or Special
A-1	

Approved for public release; distribution unlimited

PREFACE

This thesis is concerned with investigating the detection of atmospheric carbon dioxide at various temperatures and altitudes from a shuttle-borne differential absorption lidar. Absorption is from the (11'0-03'0)_I CO₂ band, and closely parallels the earlier frequency recommendations of Dr. C.L. Korb of the NASA/Goddard Space Flight Center.

I would like to thank my advisor, Maj. James J. Lange, for his patience, interest, and direction in the completion of this thesis. I would like to thank Dr. W.B. Roh, Dr. E.A. Dorko, and Dr. R.L. Hengehold for their input in resolving various problems that I encountered.

Robert H. Wank

Contents

	Page
Preface	ii
List of Figures	vi
List of Tables	vii
Abstract	viii
I. Introduction	1
Problem	2
General Approach	2
Assumptions	2
II. Atmospheric Carbon Dioxide	4
III. Structure of Carbon Dioxide	8
IV. Lidar Detection of Carbon Dioxide	13
Lidar Concept	13
Lidar Equation Computations	17
Mie and Rayleigh Scattering	27
Extinction Due to Atmospheric Absorption	31
Carbon Dioxide "On"-Resonance Cross Section	35
Carbon Dioxide "Off"-Resonance Cross Section	37
Carbon Monoxide Cross Section	37
Water Vapor Cross Section	41
Ozone Cross Section	43
Extinction Coefficient Calculations	44

	Page
Extinction Coefficient of "Off"- Resonance CO ₂	46
Extinction Coefficient of Carbon Monoxide . .	48
Extinction Coefficient of Ozone	49
Extinction Coefficient of Water Vapor	51
Calculation of "Off"-Resonance Return Signal Power	52
Background Noise Calculations	54
Signal-to-Noise Calculations (Direct Detection)	60
Heterodyne Detection	63
Detection of Hot CO ₂ in the Atmosphere	72
V. Error Analysis of DIAL Calculations	78
VI. Conclusions and Recommendations	86
Conclusions	86
Recommendations	87
Bibliography	88
Appendix A: Rayleigh Scattering Coefficients	95
Appendix B: Mie Scattering and Extinction Coefficients (4.86μ)	97
Appendix C: CO ₂ Absorption Cross Section ("On")-Resonance	99
Appendix D: CO ₂ Absorption Cross Section ("Off"-Resonance)	100
Appendix E: CO Absorption Cross Section ("Off"-Resonance)	101

	Page
Appendix F: H ₂ O Absorption Cross Section ("Off"-Resonance)	102
Appendix G: O ₃ Absorption Cross Section ("Off"-Resonance)	107
Appendix H: CO ₂ Extinction Coefficient ("Off"-Resonance)	114
Appendix I: CO Extinction Coefficient ("Off"-Resonance)	116
Appendix I: O ₃ Extinction Coefficient ("Off"-Resonance)	118
Appendix K: H ₂ O Extinction Coefficient ("Off"-Resonance)	119
Appendix L: Hot CO ₂ Absorption Cross Section ("Off"-Resonance)	120
Vita	122

List of Figures

<u>Figure</u>		<u>Page</u>
1.	Coriolis Forces in Linear CO ₂	11
2.	Classical Motion of Nuclei in Linear CO ₂ . .	11
3.	Simplified Diagram of the Differential Absorption and Scattering LIDAR Technique .	21
4.	Block Diagram of a Laser Radar With Heterodyne System	65

List of Tables

<u>Table</u>		<u>Page</u>
I.	Backscattering Coefficient and Returned Power at "Off"-Resonance	55
II.	Ideal $\left(\frac{S}{N}\right)_2$ for Heterodyne Detection	69
III.	Actual $\left(\frac{S}{N}\right)_{H2}$ for Heterodyne Detection . . .	71
IV.	Maximum Hot CO ₂ Concentration for $\left(\frac{S}{N}\right)_{H2} = 2$	77
V.	Standard Deviation of N _{CO2} at Various Altitudes	85

Abstract

Remote sensing of atmospheric carbon dioxide from a shuttle-borne differential absorption lidar (DIAL) was investigated. The investigation followed the basic frequency recommendations of Korb*, which included "on"-resonance frequency at the P(34) line of the (11'0-03'0)_I absorption band of CO₂. Extinction coefficients for CO₂, H₂O, CO, O₃, Rayleigh, and Mie scattering were determined to compute estimated return signal strengths from various altitudes. Direct detection was found to be unsuitable, but heterodyne detection provided adequate signal-to-noise ratios. Cross sections for hot CO₂ were also calculated, and maximum detectable CO₂ concentrations were determined. Finally, an error analysis of predicted CO₂ concentrations was made, which determined that due to the large CO₂ "on"-resonance extinction coefficient, accurate measurements of CO₂ below five kilometers could not be made.

*Korb, C.L. et. al. "A Lidar Technique for Measurement of Atmospheric Carbon Dioxide," Proceedings of the Tenth International Laser Radar Conference. 105-106. Silver Springs, Maryland: Committee on Laser Atmospheric Studies, October 1980.

DETECTION OF ATMOSPHERIC CARBON DIOXIDE FROM A SHUTTLE-BORNE LIDAR

I. Introduction

Atmospheric carbon dioxide (CO_2) has been gaining significantly in abundance at various monitored locations since the turn of the century (Ref. 6:2). Only recently, however, have scientists questioned the long-range environmental impact of this increase. Data is not currently available that identifies global abundance trends, major sources and sinks of CO_2 , and transport characteristics at different altitudes. In 1979, the NASA Atmospheric Lidar Working Group submitted a report (Ref. 7) detailing 26 candidate experiments for shuttle-borne lidar system, one of which recommended the measurement of the CO_2 mixing ratio at different altitudes.

Little actual measurement of CO_2 has been accomplished using a long-range lidar system. Remsberg and Gordley (Ref. 15) have analyzed the detection of several atmospheric constituents in both the troposphere and stratosphere from a shuttle-borne system, predicting only water vapor profiles as attainable in the troposphere. Korb (Ref. 17) has proposed an aircraft lidar operating at 4.86μ using a frequency-doubled CO_2 laser to measure CO_2 concentrations in the lower atmosphere.

Problem

The problem of this thesis is to investigate different lidar systems as possible candidates of a shuttle-borne system designed to measure CO₂ concentrations at various altitudes and temperatures. The analysis is directed toward applying the same general design parameters suggested by Korb in his presentation.

General Approach

The investigation centers on possible lidar systems capable of providing data from a shuttle-borne system. Using typical shuttle lidar power and optics parameters, and the suggested lidar frequencies of Korb, returned signal powers are calculated for various altitudes. Signal-to-noise calculations are then made for each altitude. Hot CO₂ concentrations are introduced below two kilometers, and a maximum detectable CO₂ concentration is determined. Finally, an error analysis of the predicted CO₂ concentrations is completed.

Assumptions

The atmosphere is considered to be nonturbulent without cloud cover. Visibility is considered to be 23 kilometers or a light haze.

Water vapor and ozone concentrations are taken from the mid-latitude model of the U.S. Standard Atmosphere, 1976 (Ref. 39).

Aerosol concentrations are derived from the model by Shettle and Fenn (Ref. 25).

II. Atmospheric Carbon Dioxide Effects

Carbon dioxide (CO_2) constitutes approximately 330ppm of the atmosphere by volume (Ref. 1:14). Along with CO , N_2O , CH_4 , and O_2 , it is generally considered a uniformly mixed gas, or one that closely maintains that 330ppm concentration over vertical profile up to about eighty kilometers. Junge and Hagemann are commonly cited for their studies in this area (Ref. 2:7). However, Manquero (Ref. 3:3) reported in September 1975 variations of a CO_2 vertical profile up to 10ppm, and Hinkley (Ref. 4:15) cites CO_2 concentrations in urban areas as high as 550ppm close to the earth's surface.

Though CO_2 is not a toxic gas, it is the only gas or liquid by-product of burning fossil fuels that has been retained in large quantities in the atmosphere (Ref. 5:9). In fact, experts have estimated that CO_2 concentrations have increased from fifteen to twenty percent since the turn of the century (Ref. 6:2), and production of CO_2 continues to increase at a 4.3 percent annual rate (Ref. 5:17). The long range effects of increased CO_2 in the atmosphere are purely speculative. Numerous models have been developed concerning the climatic consequences of changes in the temperature patterns around the world. The most common theory suggests that an increased CO_2 concentration will result in a general warming of the lower atmosphere and a

cooling of the stratosphere. This will occur due to absorption of the earth's infrared radiation by CO₂, and subsequent emission of a portion back into the atmosphere. This radiation trap is known as the "greenhouse effect" (Ref. 6:38).

One climatic model predicts doubling the CO₂ concentration will create a global temperature increase of 1.5° to 4°C by the first half of the next century, an increase considerably greater than any resulting from natural causes over the past several thousand years (Ref. 6:45). Another model predicts a temperature increase from 1°C by 2020 to and 11°C increase by 2075 (Ref. 5:23).

Kellogg (Ref. 6:4) has listed several possible consequences of a global temperature increase:

1. Middle latitude communities will require less energy demand in the winter, but more in the summer.
2. A 1°C change could add ten days to the growing season, and increased CO₂ could enhance the photosynthesis process. However, pest losses, already at 25 percent, would likely increase.
3. Natural ecosystems would shift, as some species would die out, and others migrate to new areas.
4. Precipitation patterns would shift, decreasing rainfall in the Midwest of the U.S., and the U.S.S.R., while aiding several semi-arid developing countries.

5. Climatic changes could shift ocean currents, sea surface temperatures, and wind patterns, altering the fishing industry production.
6. Labor production would decrease 2 to 4 percent for every 1°C over 20°C, and diseases previously confined to the tropics could spread to temperate regions.
7. Melting of the polar ice caps, and the subsequent rise of the oceanic levels could severely affect tourism, and result in major population shifts. For instance, a five meter rise would affect eleven million people living on the Atlantic and Pacific coasts.

Whether or not any of these predictions will actually occur is not known. Climatic models have not been developed that are sophisticated enough to consider all possible long and short range factors, due mainly to the lack of adequate atmospheric data. Predicting changes to the atmospheric CO₂ concentration requires investigation of both sources and possible sinks. Major sources of CO₂ emission include fossil-burning plants, cement manufacturing facilities, and possibly major CO₂ laser facilities. The CO₂ transport process is not yet fully understood. Of all the estimated CO₂ produced by fossil-fuel burning during a given time period, about 50 percent may actually be retained

in the atmosphere (Ref. 7:11). Others estimate that the oceans previously absorbed up to 45 percent of all CO₂ emissions, and forests almost all of the remainder. However, deforestation has resulted in the oceans being required to serve as a sink for up to 80 percent of the CO₂ emissions, a percentage they are unable to adequately absorb (Ref. 6:37).

Developing an accurate climatic model is necessary to determine whether CO₂ control measures should be imposed. Any control should be carefully evaluated since costs will be extensive. For example, it has been estimated that to remove 50 percent of CO₂ emissions from a conventional coal-fired plant would reduce the power generation efficiency from 34 percent to 25 percent, and double the cost. Removing 90 percent of CO₂ emissions would decrease efficiency to 6 to 15 percent, and increase the cost by a factor of four to seven percent (Ref. 8:iii). However, a sophisticated climatic model can only be developed with accurate knowledge of CO₂ sources, sinks, and transport processes.

III. Structured of Carbon Dioxide

Carbon dioxide (CO_2) is a linear triatomic molecule. The electronic absorption spectrum is in the far ultra-violet, unavailable for atmospheric study, and no pure rotational spectra exists due to a lack of dipole moment. For a triatomic linear molecule normal motions include three translational modes, two rotational modes (degenerate), and four vibrational modes. The available energy bands are a function of three vibrational quantum numbers describing the four vibrational modes:

1. v_1 - symmetric stretch motion.
2. v_2 - bending motion (degenerate).
3. v_3 - asymmetric stretch motion.

However, the symmetric stretch vibration (v_1), is optically inactive because the symmetry of its dipole moment is constant during vibration. The main v_2 and v_3 vibrational-rotational bands are located at approximately 667.40cm^{-1} (15μ) and 2349.16cm^{-1} (4.3μ), respectively. Overtones, hot bands, and other frequency combinations result in additional bands centered at 10.4, 9.4, 5.2, 4.3, 2.7, 2.0, 1.6, 1.4 microns, and several weak bands from .78 to 1.24 microns (Ref. 4:36).

However, it is insufficient to describe the energy levels based solely on three vibrational quantum numbers, and the rotational quantum number (J). Two additional

quantum numbers, l and r , are necessary to account for energy level shifts due to the molecule's rotational direction with respect to the vibrational bending motion, Coriolis forces, and Fermi resonance. The quantum number l accounts for the contribution of the bending mode to the angular rotation, and has values of $l = v_2, v_2-2, \dots 0$. If a molecule does not rotate, it vibrates with exactly the same frequency for the two bending modes. However, rotation about an axis affects the moments of inertia of the two modes differently so the bending frequencies are no longer equivalent. In addition a fictitious, but necessary force must be introduced in order to study a rotating coordinate system while disregarding the rotation. This is the Coriolis force and is equivalent to $\bar{F} = 2\bar{V} \times \bar{W}$, where \bar{W} is the vector angular velocity of rotation of the coordinate system, and \bar{V} is the vector velocity of motion through the coordinate system (Ref. 9:30). Vibrational frequencies ν_1 and ν_3 are excited by Coriolis forces when the bending vibration is perpendicular to the angular momentum \bar{J} . If the bending vibration is parallel to \bar{J} , no additional vibrational modes are excited since the Coriolis force is zero (See Figures 1 and 2). Because of these two effects the two degenerate bending energy levels are slightly split, which is called l -type doubling. The two sets of levels are designated \underline{c} and \underline{d} having

different rotational constants. When $l = 1$, the splitting is the most important. McClatchey (Ref. 10:11) states that:

When the linear molecule has a center of symmetry (as CO_2) with a ^{16}O at both ends, the paired atoms zero nuclear spin cause zero statistical levels of a given parity.

This means that for the ground vibrational level and all other levels with $l = 0$ and $v_3 = \text{even}$ (Π_g^+ symmetry), only even-numbered J values are found. When $l = 0$ and $v_3 = \text{odd}$ (Σ_u^- symmetry), only odd J values exist. If l is greater than zero, the \underline{c} and \underline{d} levels have different symmetry. For example if $l = 1$ (Π_g) the \underline{c} sublevel has odd levels of J , and \underline{d} has even.

The rotational constant (Ref. 9:25) for a linear molecule can be evaluated from

$$B = B_e - \sum_i \alpha_i \left(v_i + \frac{d_i}{2} \right) - J(J+1)D \quad (1)$$

where

B_e = equilibrium value of the rotational constant

α = change in B_e due to excitation of i^{th} vibration

D = change in B_e due the centrifugal stretching.

Normally, α_i can be determined by the separation of lines of adjacent vibrational states. However, perturbations between vibrational states invalidate this simple relationship. Fermi initially explained that these

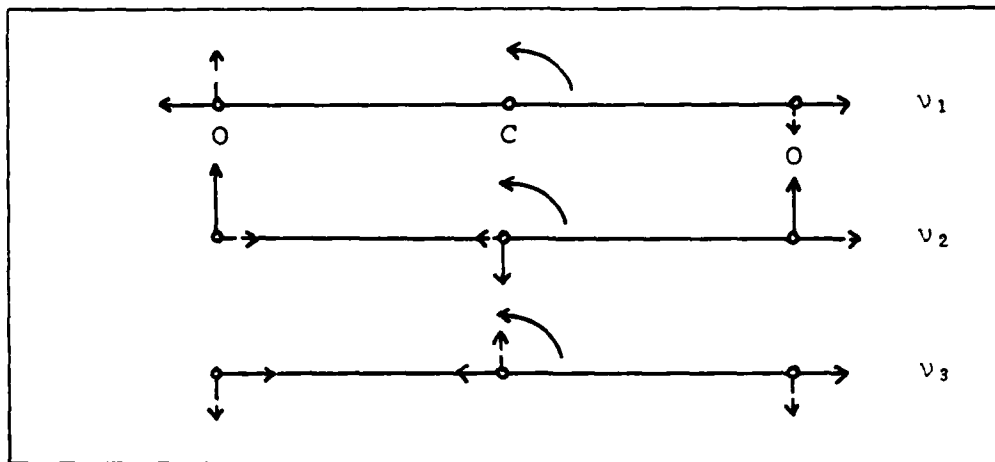


Figure 1: Coriolis Forces in Linear CO_2 - The curved arrow indicates the direction of rotation (Ref. 50:374).

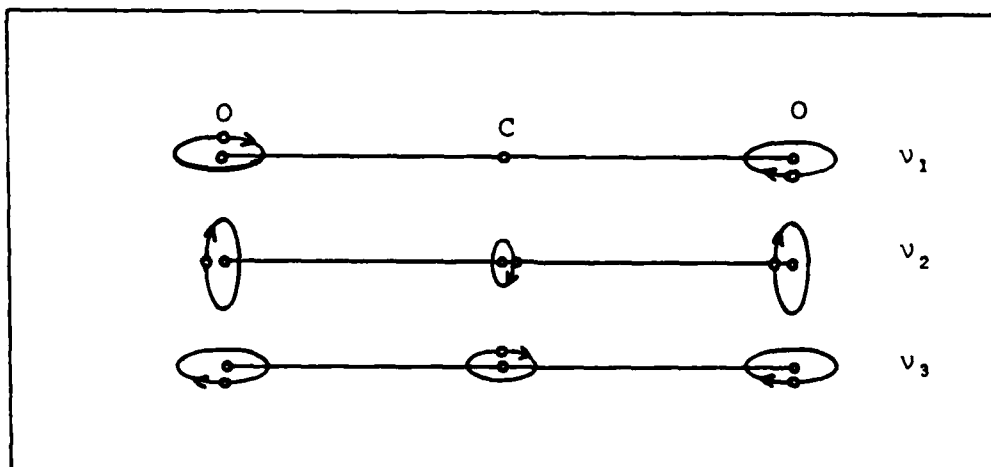


Figure 2: Classical Motion of Nuclei in Linear CO_2 (Ref. 50:375).

perturbations were due to interactions or mixing of states having similar energies, now commonly called "Fermi resonance". This necessitated introduction of a fifth quantum number, r .

This particular study will deal with the 4.86μ region of the CO_2 spectra. The region is dominated by a transition from ground state to the $(11^0, 03^0)_I$ level of the Fermi diad $(11^0, 03^0)$, where the notation follows Amat and a vibrational energy level is described as $(v_1 v_2^1 v_3)$ with a Roman numeral indicating r , the Fermi resonance level (Ref. 11:134). The band center for this vibrational energy level is located at approximately 2076.854cm^{-1} . Additional rovibrational transitions are given by

$$\begin{aligned} \hat{\sigma}(\text{cm}^{-1}) = & (E' - E''_0)/hc + B'[J'(J' + 1) - 1'^2] \quad (2) \\ & - D'[J'(J' + 1) - 1'^2]^2 - B''[J''(J'' + 1) - 1''^2] \\ & + D''[J''(J'' + 1) - 1''^2]^2 \end{aligned}$$

where

B = Rotational constant

D = Rotational constant representing the effects of centrifugal stretching.

The band is a perpendicular-type since $l = 1$, and therefore a Q-branch does exist. Also, two hot bands $(20^0, 04^0)_I - 01^0$ and $(12^2, 04^2)_I - 01^0$ have band centers located at about 2129.761 and 2093.350, respectively.

IV. Lidar Detection of Carbon Dioxide

Lidar Concept

In September 1977 a working group was convened by NASA to, among other goals, identify areas of theoretical and laboratory research necessary to support the planned development of a space shuttle-borne atmospheric lidar (Ref. 7:iii). One of the areas suggested for investigation was the CO₂ mixing ratio in the troposphere.

A lidar (light detection and ranging) operates very similar to a radar, except wavelengths vary from the near UV to the middle IR. A lidar system is commonly composed of a laser operating on a specific wavelength, whose beam propagates through the atmosphere, and is subsequently recaptured by a detection system. A lidar system can have the detector located with the laser (single-ended system) or at another location (double-ended). A spaceborne system would be single-ended. By analyzing the returned laser signal, numerous atmospheric properties can be determined. These include aerosol and thin cloud detection, temperature profiles, water vapor concentrations, trace gas detection, and wind velocity profiles. In addition, spaceborne lidar has the ability to obtain global-scale data of high spatial resolution in a short time period. Pulsed lidar, has an inherent range resolution capability, enabling three-dimensional depiction of an atmospheric target, a feature, very difficult to accurately obtain from a passive system.

Lidar systems are not new. Numerous types exist that have been successfully built and tested. Types can be divided into two categories, direct and indirect scattering. Direct scattering includes a basic lidar to measure aerosol scattering in the atmosphere, Raman lidar, and resonance (fluorescence) lidar. Indirect scattering includes differential absorption lidar (DIAL) or differential absorption scattering lidar (DAS), and additional types of Raman lidar.

Raman lidar involves the detection of molecular scattered Raman-shifted wavelengths. The scattered radiation is unique to the particular molecule being studied, and the intensity is directly proportional to the concentration. Raman lidar was first demonstrated by Kobayasi and Inaba (Ref. 12:139) to detect SO_2 and CO_2 from an oil smoke plume using a Q-switched ruby laser. However, a Raman signal is directly proportional to the Raman backscatter cross section, which typically is about $10^{-31} \text{ cm}^2 \text{ sr}^{-1}$. Therefore, it is not useful at ranges typical from a space platform to the troposphere.

Resonance lidar utilizes a pulsed laser tuned on an absorption line of the molecule being investigated to excite the molecule into a higher energy state. The molecule subsequently fluoresces with a known quantum yield at a particular wavelength, which is detected and analyzed. The cross section for a resonance interaction can be several magnitudes greater than a Raman cross section, making it suitable

for spaceborne lidar application. McIlrath has suggested the following species possibly suitable for investigation by fluorescence lidar: Li, Na, K, Ca+, Fe, Cl, O, OH, NO, BaO, and NO₂V (Ref. 13:495). In addition, Kweder has proposed HF and I₂ as promising candidates for study (Ref. 14:81). The only real disadvantage of this technique is the problem of quenching. Since an excited state has a definite lifetime, non-radiative collisions between that molecule and additional atmosphere constituents decrease the number of actual radiative decays, which affect the sensitivity and accuracy of the return signal and subsequent concentration measurement. In fact, Remsburg and Gordley in their space shuttle lidar analysis state that the fluorescence technique would be valuable only at altitudes in the upper stratosphere (Ref. 15:624), a conclusion also reached by McIlrath in his investigation of OH (Ref. 13:497).

The only technique considered feasible for tropospheric study of molecules is the differential absorption lidar (DIAL). This lidar uses a tunable laser or two separate lasers that provide electromagnetic radiation at two distinct wavelengths, one on a resonance absorption line, and the other adjacent, but tuned off that absorption line. Using a remote reflection such as the earth, the two signals are returned to a detector and analyzed. By comparing the two signal intensities, an average concentration over the

path can be determined. If molecules or aerosols serve as scattering surfaces for the two laser beams, a vertical profile of the pollutant being studied can be made. This three-dimensional technique is called range-resolved differential absorption lidar. This technique would appear to be the only suitable method available to measure the vertical distribution of CO_2 , and, therefore, will be used during this study.

Several studies of possible DIAL experiments from a space platform have been made. In fact, Remsburg and Gordley predict the only important gaseous constituent in the troposphere able to be accurately measured is the water vapor (Ref. 15:629). However, this study will investigate CO_2 concentrations using the $4.82\mu\text{m}$ band, which has been successfully used on two separate investigations. First, the Air Force Geophysics Laboratory NKC-135A Infrared Flying Laboratory conducted detailed spectral solar transmissivity studies in 1970 over Johnston Island at various altitudes in the $4.0\text{--}5.3\mu$ region demonstrating the 4.86μ band was clearly distinguishable over absorption by other atmospheric constituents (Ref. 16:2454). In 1980 Korb proposed using a frequency-doubled CO_2 laser to investigate CO_2 concentrations from an aircraft platform (Ref. 17:105). This report

parallels closely the basic physical parameters set forth in the Korb report. These include the following facts:

1. The "on" absorption line in the $(11'0, 03'0)_I - (00^{\circ}0)$ band is the P(34) line located at 2050.568cm^{-1} . To operate on this line, a frequency-doubled pulsed CO_2 TEA laser tuned to the P(42) line (2050.596cm^{-1}) of the $(00^{\circ}1) - (02^{\circ}0)$ band can be used.
2. The "off" absorption line is provided by a frequency-doubled pulsed $^{13}\text{C}^{16}\text{O}_2$ isotope TEA laser operating on the (R14) line at 2057.024cm^{-1} . This particular line was selected, because absorption by interfering species other than CO_2 was determined to be the same for both "on" absorption lines and "off" absorption lines.
3. A GdGeAs_2 crystal is used as the frequency doubling material with an efficiency of ten percent.

Lidar Equation Computations

The basic lidar equation has been derived, and tested in numerous articles and experiments. Probably the most complete derivation has been done by Measures (Ref. 18:1092) whose derivation has the flexibility to be

applicable to Raman, fluorescence, and DIAL lidars. The lidar equation utilizes the Bouguer's (Beer's) Law (Ref. 4:49):

$$I(\lambda) = I_0(\lambda) \exp[-N\sigma(\lambda)L] \quad (3)$$

where:

$I_0(\lambda)$ = Initial radiance (watts/m² - sr) of a monochromatic signal of assumed plane wave.

$I(\lambda)$ = Final radiance (watts/m² - sr) of the signal measured at a distance, L.

N = Concentration (1/m³) of absorbing species assumed uniform across L.

$\sigma(\lambda)$ = Absorption cross-section of the species wavelength, λ .

This law assumes that $\sigma(\lambda)$ is independent of both the incident radiation intensity and the concentration of absorbing molecules, N.

This report will use a combined terminology of Thompson (Ref. 19:4), Hinkley (Ref. 4:76), and the European Space Agency (Ref. 20:57). The lidar equation for DIAL measurements is as follows:

$$P_{ij}(r) = \frac{P_o \frac{c}{2} \tau_{ij}(r) A_r K E}{R_j^2} \exp \left[-2 \int_0^{R_j} \left(\xi_i(r) + N_{CO_2}(r) \sigma_i(r) \right) dr \right] \quad (4)$$

where:

- P_{ij} = Returned power signal (watts) from range r at time t .
- i = Subscript denoting the wavelength of the laser where $i = 1$ is "on" absorption line and $i = 2$ is "off".
- j = Subscript denoting vertical range cell under investigation.
- P_0 = Transmitted power at time t_0 (watts).
- c = Velocity of light in vacuum.
- τ = Integration time of the returned power signal (sec).
- $\beta_{ij}(r)$ = Volumetric backscattering coefficient of the atmosphere ($\text{km}^{-1}\text{sr}^{-1}$).
- A_r = Effective receiver area (km^2).
- R_j = Range from the space shuttle to the range cell under investigation.
- $\xi_i(r)$ = Extinction coefficient of atmosphere minus extinction due to CO_2 (km^{-1}).
- $N_{\text{CO}_2}(r)$ = Number density of CO_2 molecules (km^{-3}).
- $\sigma_i(r)$ = Absorption cross section of CO_2 (km^2).
- K = Transmittance of the optics of the return signal.
- e = Frequency-doubling crystal efficiency and Transmittance of the optics for the outgoing signal.

The integration time, τ , is selected based on the desired vertical size of a range cell. The size of a cell is given by $\frac{c\tau}{2}$ (See Figure 3). A cell size of 1km has been selected for this study. The initial signal power is determined from $P_0 = \frac{U_0}{\tau}$ where U_0 is the energy in joules and the τ the pulse duration. For use on a space shuttle, the NASA Atmospheric Lidar Working Group suggested a TEM₀₀ pulsed CO₂ laser with energy from 1-10 joules at 1-50Hz with a 150ns pulse (Ref. 7:172). Brockman, in his analysis of O₃, H₂O, and NH₃ measurements by a pulsed CO₂ spaceborne lidar uses an energy of 5 joules with 1000 shots (Ref. 21:564). Megie and Menzies in their UV and IR DIAL comparison study assume a pulsed CO₂ laser with an energy of 2 joules, 100n sec pulse duration with a 10Hz repetition rate (Ref. 22:1181). This study will use Megie and Menzies' parameters. Generally, the telescope receiver diameter is assumed to be 100cm for a space shuttle lidar with an optical system efficiency of 30 percent. The frequency-doubling crystal efficiency is assumed to be 10 percent.

The term $\exp -2 \int_0^R (\xi_i + N_{CO_2} \sigma_i) dr$ is the fractional transmittance of energy along a two-way path between the lidar and the range cell. The total extinction coefficient minus CO₂ absorption (ξ_i) can be divided into three components:

1. $\xi_{ik}(\lambda)$ = Extinction coefficient due to continuum absorption.

2. $\xi_{is}(\lambda)$ = Extinction coefficient due to Mie and Rayleigh scattering.

3. $\xi_{ia}(\lambda)$ = Extinction coefficient due to selective absorption, which is highly wavelength dependent.

Equation (4) is the generally accepted form for the DIAL equation. However, this form assumes a laser of monochromatic frequency, when in fact, the laser has a definite line shape. For a CO₂ TEA laser operating at one atmosphere, the full width at half maximum frequency is approximately 4.2GHz at 300°K, or .14cm⁻¹ (Ref. 52:17) with a Lorentzian line shape. Therefore, a more correct statement for the returned signal power must include a convolution of the absorption and laser line shapes, given as follows:

$$P_{ij}(r, \lambda) = \int_0^\infty P_{\lambda ij}(r, \lambda) d\lambda = \frac{\frac{c}{2} \tau A_r K e}{R_j^2} \int_0^\infty P_{o\lambda}(\lambda) s_{ij}(r, \lambda) \exp \left[-2 \int_0^{R_j} \left(\xi_i(r, \lambda) + N_{CO_2}(r) \sigma_i(r, \lambda) \right) dr \right] d\lambda$$

Even considering that $s_{ij}(r, \lambda)$ is not highly wavelength sensitive in the infrared, the remaining integral is very difficult to evaluate analytically or numerically. Therefore, this study will assume that the additional error

introduced by neglecting the shape of the laser pulse will not significantly alter the final results. This has been assumed extensively in the past giving mixed results when theoretical extinction coefficients are compared to actual experimental results. For example, several studies have been done on DF and CO laser attenuation at various atmospheric pressures, temperatures, and compositions. These studies around 5μ should give an indication on whether the attenuation of a laser in that region for this study can be approximated by Equation (4).

For the DF laser, theoretical calculations of extinction coefficients due to N_2O , CO, O_3 , N_2 , and aerosols were initially done by McClatchey and Selby (Ref. 53:2) in 1972 using a simple Lorentzian line shape for the interfering species to determine the attenuation. Several studies have been done to experimentally confirm or refute these calculations. Mills, in his very complete theoretical and experimental study in 1976 (Ref. 54:108), compares his experimental results of DF laser attenuation by N_2 and those of two other experiments to the calculated extinction coefficients of N_2O assuming absorption cross sections with a simple Lorentzian line shape. His results compare very favorably (1 or 2 percent discrepancy) with theoretical calculations. While the other two studies do not agree as well, extrapolation of the data is considered the primary reason, and not the theoretical technique. Mills also cites

studies by Myers of attenuation of the DF laser by CO_2 , which had discrepancies up to four orders of magnitude from the theoretical, and assumed to be caused by a weak CO_2 band not included in computations (Ref. 54:121). Mills also compares his experimental attenuation of DF laser radiation due to H_2O to the combined attenuations of calculated H_2O plus continuum H_2O absorption calculations of Burch (Ref. 54:143). The simple Lorentzian line shape for absorption again gave generally good results with a maximum of 40 percent error. Finally, Deaton investigated DF laser attenuation by methane (Ref. 55:302). Results indicated that theoretical attenuation predictions were up to two orders of magnitude less than actual experimental results. This was explained by the theoretical calculations considering only eight strong methane absorption lines between 2710.96 and 2712.11cm^{-1} , when actually 71 lines lying between 2700 and 2720cm^{-1} all contributed to the total absorption.

For attenuation of CO laser radiation, McClatchey again did the first major theoretical calculations, which he based on a monochromatic CO laser using a simple Lorentzian absorption line shape (Ref. 56:7) for attenuation by H_2O , CO_2 , O_3 , CH_4 , and aerosols. This was followed by a study by Ford (Ref. 57:37), who analyzed the parameters of CO laser attenuation particularly effects of water vapor and attenuation at the extreme wings using a simple Lorentzian absorption line shape. This study was continued, comparing Ford's

experimental results of CO laser attenuation by H_2O at four different pressures to calculated attenuations (Ref. 58:12). Generally, results were quite close, with any discrepancies caused by failure to consider absorbing lines or effects of extreme wings. Long followed up this study with additional results in 1973 (Ref. 59:34). His data showed that the attenuation of CO laser radiation predicted by the simple Lorentzian line shape of H_2O molecules gave consistently lower values than experimental values of extinction coefficients. A second line shape was derived to account for the additional absorption which was due to absorption in the extreme wings.

These studies of CO and DF laser radiation clearly indicate that even though the laser line shape has not been considered in the past, accurate results of predicted laser attenuation can be made. Any discrepancies between experimental results and theoretical calculations appear to be due to failure to consider weakly absorbing lines, absorption in the extreme wings, and the inadequacy of the simple Lorentzian line shape to describe extreme wing effects correctly. However, adding a factor to approximate the line shape of the laser can only confuse the situation, and may, in fact, lead to more inaccurate results. Therefore, this study will continue to use the convention for the DIAL equation given in Equation (4).

In order for a return signal (P_{ij}) to be detectable two conditions must be met (Ref. 20:59):

1. $P_{1j} \geq P_n$ where P_n is the equivalent noise power of the system.
2. $P_{2j} - P_{1j} \geq P_n$

If it assumed that $\xi_1 = \xi_2$ as previously stated from the Korb study, then Equation (4) yields:

$$P_{2j} \exp \left[-2 \int_0^{R_j} N_{CO_2} \Delta\sigma dr \right] = P_{1j} \quad (5)$$

where $\Delta\sigma = \sigma_1 - \sigma_2$

Therefore, the first condition above yields:

$$P_{2j} \exp \left[-2 \int_0^{R_j} N_{CO_2} \Delta\sigma dr \right] \geq P_n \quad (6)$$

However, the power signal-to-noise ratio is defined as on the "off" absorption wavelength:

$$\frac{P_{2j}}{P_n} = \left(\frac{S}{N} \right)_2 \quad (7)$$

Combining Equations (6) and (7) yields:

$$\exp \left[-2 \int_0^{R_j} N_{CO_2} \Delta\sigma dr \right] \geq \frac{1}{(S/N)_2} \quad (8)$$

The second condition above combined with Equation (5) gives:

$$P_{2j} - P_{2j} \exp \left[-2 \int_0^{R_j} N_{CO_2} \Delta\sigma dr \right] \geq P_n \quad (9)$$

Combining with Equation (7):

$$\left(\frac{S}{N}\right)_2 \geq \frac{1}{1 - \exp \left[-2 \int_0^{R_j} N_{CO_2} \Delta \sigma dr \right]} \quad (10)$$

This can be rewritten into the more useful form:

$$\exp \left[-2 \int_0^{R_j} N_{CO_2} \Delta \sigma dr \right] \leq 1 - \frac{1}{(S/N)_2} \quad (11)$$

Combining Equations (11) and (8) yields:

$$1 - \frac{1}{(S/N)_2} \geq \exp \left[-2 \int_0^{R_j} N_{CO_2} \Delta \sigma dr \right] \geq \frac{1}{(S/N)_2} \quad (12)$$

In order to satisfy both conditions of detectability it can be seen that $\left(\frac{S}{N}\right)_2$ must equal two as a minimum. Therefore, it is necessary to evaluate P_{2j} and P_n to determine whether the parameters of this particular lidar are acceptable to detect atmospheric CO_2 .

Mie and Rayleigh Scattering

Rayleigh scattering is classical, elastic scattering involving incident electromagnetic radiation and atmospheric molecules. No appreciable loss of energy occurs, and the frequency is not changed. Since all molecules contribute to Rayleigh scattering, conclusions about concentrations of individual constituents cannot be made. The extinction coefficient due to Rayleigh scattering is given by (Ref. 4:52):

$$\xi_{iR}(\lambda) = [8 \pi^3 (n^2 - 1)^2 / 3 N_g \lambda^4] [(6 + 3\delta) / (6 - 7\delta)] \quad (13)$$

where:

N_g = Number density of gas molecules.

n = Refractive index of the medium.

δ = Depolarization factor of scattered radiation $\approx .035$.

λ = Wavelength of incident radiation.

Note the λ^{-4} dependence. Experiments with several atmospheric models has yielded a simple empirical equation for the cross section due to Rayleigh scattering up to an altitude of 100km (Ref. 4:98):

$$\sigma_{iR}(\lambda) = 4.56 (\lambda(\mu) / .55)^{-4} \times 10^{-27} \text{ cm}^2 \quad (14)$$

Since $\xi_{iR} = N_g \sigma_{iR}$, the Rayleigh extinction coefficient can be calculated for various altitudes, using number densities from a U.S. Standard Atmosphere (Ref. 23:6). See Appendix A for computations. After calculating the extinction coefficient, the volumetric backscattering coefficient (β_{ijR}) due to Rayleigh scattering can be computed. β_{ijR} is a measure of the amount of radiation scattered into a solid angle from a given volume of gas. The magnitude of β_{ijR} is given by the Rayleigh scattering law (Ref. 20:24):

$$\beta_{ijR} = \xi_{iR} (3/8\pi) \quad (15)$$

Mie scattering requires a much more complex model. It involves interaction between electromagnetic radiation, and particles of size approximately equal to or larger than the wavelength of the radiation. Particle size can range from $10^{-3}\mu$ for the dust or pollen to $10^4\mu$ for raindrops. Size of particles particularly affects the angular distribution of scattering (Ref. 1:70). The interaction, dominated by elastic scattering, also includes an absorption component. An additional significant factor, besides wavelength and particle size distribution, is refractive index of the particle. Due to the complex nature of Mie scattering, the general approach to analyzing its effects is the use of an empirical atmospheric model. Several exist including Deirmendjian haze models (Ref. 26:187), Elterman's Atmospheric model (Ref. 23:1), a simplified LOWTRAN MODEL (Ref. 27:11), Shettle and Fenn's model of atmospheric aerosols (Ref. 25:2-1), and a simple empirical equation relating the Mie scattering coefficient to visual range:

$$\xi_{iM} = (3.91/V) (.55/\lambda)^{.585V^{\frac{1}{3}}} \text{ km}^{-1} \quad (16)$$

where V is the visual range in kilometers and λ the wavelength in microns. This equation is often used, but would be difficult to analyze for various altitudes, and the validity of its extension to the infrared from the visual spectrum has been questioned (Ref. 24:1500). For this study Shettle and Fenn's aerosol model will be used due to its

extensive experimental basis and close agreement with Elterman's model. Fenn's model does not include turbulent effects on scattering or absorption. The study divides the atmosphere into four regions:

1. A boundary layer up to two kilometers describing aerosols in a rural, urban, and maritime environment.
2. Troposphere up to about ten kilometers representing spring and summer or fall and winter conditions.
3. Stratosphere up to thirty kilometers for background, moderate, high, and extreme volcanic conditions for two seasonal models.
4. Upper atmosphere including a model with background conditions, and one with a high aerosol concentration for those altitudes.

The Shettle and Fenn model plots the attenuation coefficient versus wavelength. By combining the data from both graphs, extinction coefficients and scattering coefficients due to Mie scattering can be estimated at $4.82\mu\text{m}$. This study made the following assumptions:

1. Urban model in the boundary layer for a moderately clear atmosphere (23km visibility).
2. Only normal background is considered in the stratosphere, and volcanic effects are neglected.

3. Any attenuation over 30km is assumed to be negligible.

Results due to extinction and scattering due to aerosols can be found in Appendix B.

Extinction Due to Atmospheric Absorption

The extinction coefficient due to absorption can also be defined as:

$$\xi_i(\lambda) = N_g \sigma_i \quad (17)$$

where σ_i is the absorption coefficient for a molecule at either the "on" or "off" absorption wavelength and N_g is the number density of the particular molecule. The cross section must be determined for three different cases. First, in the lower atmosphere, collision broadening dominates and the absorption line generally takes the form of a simple Lorentzian (Ref. 4:32):

$$\sigma(\nu) = \frac{(S/\pi) \alpha_L}{(\nu - \nu_0)^2 + \alpha_L^2} \quad (18)$$

where

$\sigma(\nu)$ = Absorption line cross section (cm^2).

S = Line intensity of an individual spectral line ($\text{cm}^2 \text{ cm}^{-1} \text{ mol}^{-1}$), and $s = \int_0^\infty \sigma(\nu) d\nu$.

α_L = Half width at half maximum of the absorption line (cm^{-1}).

ν = Wavenumber (cm^{-1}) of incident radiation.

ν_0 = Wavenumber (cm^{-1}) of the line center.

Quantum mechanics provides this expression for the intensity of separate transitions of a molecule from state k into state l (Ref. 4:34):

$$S_{kl} = (8\pi^3 \nu_{kl} / 3hc) (N_k / g_k N) \left| R_{kl} \right|^2 \left[1 - \exp(-hc \nu_{kl} / kT) \right] \quad (19)$$

where

ν_{kl} = Transition wavenumber.

N_k / N = Fractional number density in state k
with statistical weight g_k .

$\left| R_{kl} \right|^2$ = Square of the matrix element of the
dipole moment.

h = Planck's constant.

c = Speed of light.

k = Boltzmann's constant.

T = Temperature of the medium.

The simple Lorentzian is not the only line shape used to describe collisional broadening. Serious problems in the extreme wings where $\left| \nu - \nu_0 \right|$ is very large has resulted in development of modifications to the simple Lorentzian such as the Gross, Van Vleck-Weisskopf, and Van Vleck-Huber line shapes (Ref. 28:9). However, none of these are totally satisfactory for extreme wing measurements. Therefore, this study will assume a collisional-broadening line shape of a simple Lorentzian.

Collisional broadening dominates below about 20 kilometers. Above 30 kilometers, however, Doppler broadening, which is independent of pressure, dominates. The absorption cross section for a Doppler-broadened line shape is Gaussian given by (Ref. 4:33):

$$\sigma(\nu) = (S/\alpha_D)(\ln 2/\pi)^{\frac{1}{2}} \exp \left[-(\nu - \nu_0)^2 \ln 2 / \alpha_D^2 \right] \quad (20)$$

where

$$\alpha_D = (\nu_0/c)(2kT \ln 2/m)^{\frac{1}{2}}$$

where

m = Mass of an individual molecule of a particular gas.

It will be shown that absorption above 30 kilometers is negligible compared to effects of the lower atmosphere.

For regions between about 20 to 30 kilometers, absorption line shapes are a convolution of the Gaussian and Lorentzian known as the Voigt line shape. The Voigt profile is given by (Ref. 4:246):

$$\sigma(\nu) = (S/\Delta\nu) \operatorname{Re} \{w(x + iy)\} \quad (21)$$

where

$\operatorname{Re}\{w(x + iy)\}$ = Real part of the error function of complex argument, $w(x)$.

$$\begin{aligned} \Delta\nu &= (\pi \ln 2)^{\frac{1}{2}} \alpha_D \\ x &= (\nu - \nu_0) \Delta\nu \\ y &= \alpha_L / \Delta\nu \end{aligned}$$

However, to simplify calculations in this study a simple Lorentzian was assumed, which is a valid assumption since almost all of the significant absorption occurs below 10 kilometers. The effect of using a Lorentzian above 20 kilometers, if anything, results in a more conservative return signal than if the Voigt profile was included.

The total extinction coefficient due to absorption is given by:

$$\xi_i = \sum_{k=1}^m \xi_{ik} \quad (22)$$

where

m = Number of absorbing species in the atmosphere.

The Infrared Handbook (Ref. 29:5-92) provides a diagram of major atmospheric constituents affecting transmission in the 4.86μ region. These include CO_2 , water (H_2O), ozone (O_3), and carbon monoxide (CO). Effects of the isotope $^{13}\text{C}^{16}\text{O}$ (1-0) band are neglected due to its small atmospheric concentration. For this same reason, effects of the ($00^{\circ}1 - 00^{\circ}0$) band of carbonyl sulfide (OCS) with a band center at 2062.2cm^{-1} (Ref. 30:1325) will be ignored. The extinction coefficient for the major absorbers listed above will be discussed individually.

Carbon Dioxide "On" - Resonance Cross Section

The basic structure of carbon dioxide has been previously discussed. A major effect of the $(11^0 - 03^0)_I - (00^0)$ band is the large Coriolis effect resulting from $l = 1$. These Coriolis-type resonances induce a large part of the transition moment in the R- and P- branches, thus "borrowing" intensity from stronger parallel bands (Ref. 10:26). Determination of actual intensities of individual absorption lines has not always been theoretically predicted or experimentally verified. Formally, the intensity of any line at wavenumber ν can be expressed as (Ref. 10:13)

$$S_m = \frac{\nu}{\nu_0} \cdot S_v^0 \cdot S_{\text{Rot}} \cdot F \quad (23)$$

where

S_v^0 = Vibrational intensity of a nonrotating molecule at a vibrational origin, ν_0

F = Factor that accounts for simultaneous vibration and rotation.

For a first order theoretical correction the F -factor can be expressed as

$$F = S_{\text{nonrigid}}/S_{\text{rigid}} = (1 + \xi_m)^2 \quad (24)$$

where

$m = (J'' + 1)$ for R-branch; $(-J'')$ for P-branch; (J'') for Q-branch.

ξ = Empirical value used by McClatchey to describe a particular vibrational band.

As further simplification for CO_2 , McClatchey used the equation below to correct for the Coriolis effect, and determine individual line intensities:

$$S_m = S_v (1 + m \xi)^2 \quad (25)$$

where for the $(11'0 - 03'0)_I - (00^00)$ band (Ref. 31:518)

$$S_v^0 = 35.9 \times 10^{-22} \text{mol}^{-1} \text{cm}^2 \text{cm}^{-1}$$

$$\xi = -.041$$

However, this expression would appear to give erroneous data for the P-branch since S_m would continue to increase as J increases. Burch (Ref. 32:4-7) completed excellent high resolution spectroscopy of this band in 1970, which confirms the predicted reduction of the R-branch, and enhancement of the P-branch. Snyder (Ref. 32:3) reported that an additional higher order term of the F-factor must be used for the $(11'0 - 03'0)_I - (00^00)$ band so

$$F = (1 + \xi_1 m + \xi_2 m^2)^2 \quad (26)$$

$$\text{and } \xi_1 = -.0237, \quad \xi_2 = -.000527$$

This analysis gives results which more accurately coincide with the spectra of Burch than the simple first order approximation. Experimental verification of individual line half-widths has not been completed. Therefore, this study

will use an average value of $\alpha_1 = .07\text{cm}^{-1}$ for one atmosphere of pressure at 296°K (Ref. 10:6). Using Equations (18) and (26) with the "on" wavenumber of 2050.596cm^{-1} , a total absorption cross section was computed: $\sigma_{2\text{CO}_2} = 2.029 \times 10^{-20}\text{cm}^2$.

Appendix C lists the individual line strengths and absorption cross sections that significantly contribute to the total absorption. Note the dominate absorption cross section of the P(34) line.

Carbon Dioxide "Off" - Resonance Cross Section

This analysis parallels closely to that of the "on" wavelength except $\nu = 2057.024\text{cm}^{-1}$, corresponding to the frequency-doubled $^{13}\text{C}^{16}\text{O}_2$ laser ($00^{\circ}1 - (10^{\circ}0, 02^{\circ}0)_{\text{II}}$ band). Again, $\alpha_L = .07\text{cm}^{-1}$. Using Equations (18) and (26), the total absorption cross section can be computed.

Appendix D lists the individual line intensities and cross sections for CO_2 at off resonance with the total $\sigma_{2\text{CO}_2} = 1.36 \times 10^{-21}\text{cm}^2$. This is approximately 15 times less than the on-resonance cross section.

Carbon Monoxide Cross Section

Carbon Monoxide (CO) is a well-studied diatomic molecule. In general for a diatomic molecule, molecular rotational transitions ($J = \pm 1$) have, to a good approximation, the same transition probability. However, absorption lines do not have the same intensity. Instead,

intensities are directly proportional to the initial number of molecules in each level (Ref. 51:II-12). The (1-0) band of CO with a band center at 2134.2716cm^{-1} , dominates the spectrum in the 4.86μ region. The band sum intensity, $\sum S_M$, is reported by Rothman (Ref. 34:793) as $981.3 \times 10^{-20}\text{cm}^{-1}\text{mol}^{-1}\text{cm}^2$. In order to determine the fraction of the total band intensity that each individual absorption line contributes, molecular number densities for each rotational level of the vibrational ground state must be computed. The relationship between the number density in a particular vibrational level to the total number density assuming a Boltzman distribution, is given by

$$\frac{n_v}{n_{\text{Tot}}} = \frac{\exp\{-E_v/kT\}}{Q_v} \quad (27)$$

where

$$E_v = hc \left[\overline{\omega}_e (v + \frac{1}{2}) - \overline{\omega}_e (v + \frac{1}{2})^2 \chi_e \right] \quad (28)$$

Q_v (vibrational partition function)

$$= \sum_{v=0}^N \exp \frac{-hc \overline{\omega}_e (v + \frac{1}{2}) - \overline{\omega}_e (v + \frac{1}{2})^2 \chi_e}{kT} \quad (29)$$

$\overline{\omega}_e$ = Hypothetical equilibrium frequency of an anharmonic oscillator and for CO has a value of 2169.74cm^{-1} (Ref. 51:V-11)

χ_e = Anharmonicity constant for a diatomic molecule and has a value of .0061 for CO (Ref. 51:III-20)

To compute Q_v it can be shown that essentially all molecules are in the ground vibrational level at a temperature of 296°K

$$\frac{n_{v=1}}{n_{v=0}} = \exp\left(\frac{\Delta E_{v=1} - v''}{kT}\right) = 3.086 \times 10^{-5} \quad (30)$$

$$\frac{n_{v=2}}{n_{v=0}} = 1.05 \times 10^{-9} \quad (31)$$

Like carbon dioxide, carbon monoxide is considered by McClatchey as a uniformly mixed gas in the atmosphere, with a number density of .075ppm. The $^{12}\text{C}^{16}\text{O}$ isotope composes 98.652 percent of the atmosphere CO (Ref. 10:6). From the U.S. Standard Atmosphere (Ref. 23:6) the total molecule number density at the earth's surface, N_{Tot} , is $2.547 \times 10^{19} \text{ cm}^{-3}$. Therefore,

$$N_{\text{Tot}}^{12}\text{C}^{16}\text{O} = 1.884 \times 10^{12} \text{ cm}^{-3}$$

All of the $N_{\text{Tot}}^{12}\text{C}^{16}\text{O}$ molecules must occupy a particular vibrational energy level, and so

$$N_{\text{Tot}}^{12}\text{C}^{16}\text{O} = n_{v=0} + n_{v=1} + n_{v=2} + \dots \quad (32)$$

Combining with Equations (30) and (31)

$$N_{\text{Tot}}^{12}\text{C}^{16}\text{O} \approx n_{v=0} (1 + 3.086 \times 10^{-5} + 1.05 \times 10^{-9})$$

$$N_{\text{Tot}} \approx n_{v=0} \approx 1.884 \times 10^{12} \text{ cm}^{-3}$$

Since essentially all of the CO molecules are in the ground vibrational state, it is now necessary to determine their distribution in the rotational levels. Again, assuming a Boltzman distribution and including the degeneracy due to angular momentum, the molecular number density of a rotational level to the total number density of that vibrational band is given by

$$\frac{n_J}{n_v} = \frac{\{(2J + 1)\exp(-E_J/kT)\}}{2Q_r} \quad (33)$$

where

$$Q_r \text{ (Rotational partition function)} \\ = \sum_{J=0}^N \{(2J + 1)\exp(-Bhc J(J + 1)/kT)\} \quad (34)$$

$$B \text{ (Rotational constant)} = 1.9225\text{cm}^{-1} \text{ (Ref. 35:207).}$$

The factor of $\frac{1}{2}$ is needed since only the P-branch of the band contributes to the absorption. Q_r must be computed for each value of J . For this study computed values for $J = 0$ to $J = 30$ were used. Values below $J = 30$ were insignificant. Summing over the 31 values gives $Q_r \approx 107.32$. Knowing the total band intensity and using Equation (33), the individual absorption line intensities can be computed from the simple proportion

$$\frac{n_J}{n_{\text{Tot}}} \sum S_m = S_m \quad (35)$$

Again, since individual absorption line half-widths are not available, an average value, α_L , of $.06\text{cm}^{-1}$ (Ref. 10:6) is used. Using Equation (18) where $\nu = 2057.024\text{cm}^{-1}$, the "off" resonance wavenumber, individual absorption cross sections can be computed. Appendix E lists these results for significantly contributing absorption lines, along with the line centers (Ref. 35:204), and line intensities. A summation of the individual line cross sections provides a total cross section of $\sigma_{2\text{CO}} = 3.585 \times 10^{-22}\text{cm}^2$.

Water Vapor Cross Section

Water has the structure of an asymmetric-top molecule, which is a rotor where no two principal moments of inertia are equal. This necessitates the use of three quantum numbers to describe a particular rotational level (J, K_a, K_c) (Ref. 10:12). K_a and K_c assume all values 0, 1, 2, . . . J, subject to $K_a + K_c = J$ or $J + 1$. Therefore, $2J + 1$ levels exist only for a given J. Also, a nuclear-spin statistical weight must be applied to all asymmetric top molecules with two or more identical nuclei. Therefore, the probability of occupation of a particular rotational level must be multiplied by a weighting factor of 3 or 1 depending on the spin of the nuclei in relation to the rotation of the molecule (Ref. 9:103). These and other complexities hinder analysis of absorption spectra. Fortunately, a recent work by Flaud and Camy-Peyret (Ref. 36)

not only lists the wavenumbers of the individual transitions by the quantum numbers J' , J'' , K_a' , K_a'' , K_c' , K_c'' , but also provides the line intensities of individual lines. There has been considerable debate regarding the variation of the absorption line half-width of H_2O . This study uses a value of $\alpha_L = .032\text{cm}^{-1}$, (Ref. 10:20). Using Equation (18) where χ = the absorption cross section for 109 individual lines was computed. Results are given in Appendix F. A summation of the individual cross sections gives $\sigma_{2H_2O} = 9.85 \times 10^{-25}\text{cm}^2$.

The actual value of the total absorption cross section due to water is actually larger due to continuum absorption. There have been four sources suggested as contributing to this additional absorption (Ref. 28:7):

1. Extreme wings of absorption lines of H_2O molecules (monomers).
2. Dimers ($H_2O:H_2O$) or H_2O molecules bound in an equilibrium state.
3. Dimers in a nonequilibrium state.
4. Uncharged clusters of H_2O molecules.

Burch (Ref. 28:20) has stated that for radiation in the 4.8μ region, continuum absorption can be ignored outside the interval from 100cm^{-1} to 2500cm^{-1} . However, this region still includes about 6200 absorption lines. He has shown that if a modified Van Vleck-Weisskopf (MVVW) line shape is used instead of a simple Lorentz, that the Lorentz

predicts at $\nu = 2056.0\text{cm}^{-1}$ only .879 of the absorption predicted by MVVW at a temperature of 308°K. However, the computed value of the total cross section is probably accurate to about a factor of two, which will not have any significant effect on the total extinction coefficient due to all of the interfering species.

Ozone Cross Section

Ozone (O_3) is also an asymmetric-top molecule, very similar in structure to water. However, the nuclear-spin statistical weight factor for isotopically symmetrical O_3 has values of 0 or 1 for the odd or even parity of $J + K_a + K_c + v_3$ (Ref. 10:12). The primary bands contributing to absorption in the 4.86μ region include the $(10^01) - (00^00)$ band, centered at 2110.785cm^{-1} with a band of strength, $\sum S_m = 113.4 \times 10^{-20}\text{cm}^{-1}\text{mol}^{-1}\text{cm}^2$, and the $(00^02) - (00^00)$ band, centered at 2057.892cm^{-1} with a band strength, $\sum S_m = 11.1 \times 10^{-20}\text{cm}^{-1}\text{mol}^{-1}\text{cm}^2$. The $(20^00) - (00^00)$ band centered at 2201.157 also contributes slightly (Ref 34:792). Again, it is fortunate that Flaud and Camy-Peyret in another study have evaluated this particular molecule, identifying transitions by the three rotational quantum numbers, their respective wave number, and the intensity of the transition (Ref 37:192). A line half-width, $\alpha_L = .11\text{cm}^{-1}$ is assumed (Ref 10:6). Again, using equation (18) with $\nu = 2057.024\text{cm}^{-1}$, individual cross sections can be calculated. Appendix G lists the wave

number, intensity, and cross section for 170 lines that contribute significantly to the total absorption cross section. Summing individual cross sections gives a total cross section of $\sigma_{2O_3} = 1.37 \times 10^{-21} \text{ cm}^2$.

Extinction Coefficient Calculations

Cross sections have been calculated for the interfering species of CO_2 , CO , H_2O , and O_3 . However, these calculations are made at 1 atm and 296°K . In fact the line intensity is a function of temperature. Therefore, if the Lorentzian line shape is valid up to 30 kilometers in altitude, cross sections as a function of altitude must be calculated. If these cross sections are known, then using Equation (17) extinction coefficients can be calculated by multiplying the cross section by the interfering species' number density as a function of altitude.

The intensity of absorption line as a function of temperature is given by McClatchey (Ref. 10:3) as:

$$S(T) = \frac{S(T_s)Q_v(T_s)Q_r(T_s)}{Q_v(T)Q_r(T)} \exp \left[\frac{1.439E''(T - T_s)}{TT_s} \right] \quad (36)$$

where

E'' = Energy of the lower state of the transition (cm^{-1}).

Q_v, Q_r = Vibrational and rotational partition functions,

$S(T_s)$ = Line intensity at the standard temperature,

$T_s = 296^\circ\text{K}$.

Tuer (Ref. 1:16) has reported the following equation relating the line half-width to temperature and pressure:

$$\alpha_L(T, P) = \alpha_L(T_s, P_s) (P/P_s) (T_s/T)^n \quad (37)$$

where

$\alpha_L(T_s, P_s)$ = Line half-width at temperature,

$T_s = 296^\circ\text{K}$, and pressure, $P_s = 1 \text{ atm}$.

$n = \frac{1}{2}$, assuming temperature independent collision diameters.

This value for n is uncertain since values have been reported up to $n = 1$. However, $n = \frac{1}{2}$ is the most commonly adopted figure, and will be used in this study.

From Equation (18) it can be seen that the absorption line cross section varies as α_L^2 varies in the denominator. However, the contribution of this term is insignificant unless the incident radiation wavenumber happens to coincide very closely with an absorption line center, as is the case when operating on the "on"-resonance laser frequency. However, when operating "off"-resonance, this factor can be ignored. Therefore, by combining Equations (18), (35), and (36), an "off"-resonance cross section as a function of temperature and pressure can be calculated from:

$$\sigma_2(P, T) = \sigma_2 \left[\frac{Q_v(T_s)}{Q_v(T)} \frac{Q_r(T_s)}{Q_r(T)} \right] \exp \left[\frac{1.439(T - T_s)E''}{TT_s} \right] \left[\frac{P}{P_s} \right] \left[\frac{T_s}{T} \right]^{\frac{1}{2}} \quad (38)$$

Extinction Coefficient of "Off" - Resonance CO₂

The vibrational band of the lower energy level of the $(11'0 - 03'0)_I - (00^{\circ}0)$ transition is ground state. The energy for a particular rotation-vibrational level for a linear triatomic molecule can be approximated as (Ref. 51:VI-6)

$$E_{v''J''} \approx B''J''(J'' + 1) + \sum_i (v_i'' + \frac{1}{2})\bar{\nu}_i \quad (39)$$

where for the ground vibrational state

$$B'' = .3902\text{cm}^{-1} \quad (\text{Ref. 11:137})$$

$$\bar{\nu}_1 = 1330.0\text{cm}^{-1}; \bar{\nu}_2 = 667.3\text{cm}^{-1}; \bar{\nu}_3 = 2349.3\text{cm}^{-1} \quad (\text{Ref. 33:VI-6}).$$

Since it would be very difficult to calculate an individual line absorption cross section as a function of altitude for each line contributing to absorption, a rotational quantum number, J'' , will be selected corresponding to the line that contributes most significantly to the total absorption. In this case that line is the P(26) line (See Appendix D), so $J'' = 26$. Using Equation (39), $E_{v''J''} = 0$, $J'' = 26 \approx 2447.23\text{cm}^{-1}$.

McClatchey (Ref. 10:4) provides the following values of $Q_v(T)$:

<u>Temp</u> (°K)	175	200	225	250	275	296
<u>Q_v</u> (T)	1.0095	1.0192	1.0327	1.0502	1.0719	1.0931

McClatchey also states that the ratio of the rotational partition functions varies as:

$$\frac{Q_r(T_s)}{Q_r(T)} = \left(\frac{T_s}{T} \right)^j \quad (40)$$

where $j = 1$ for CO_2 .

This expression is the result of an approximation of Q_r . Instead of summing over all values of J in Equation (34), integration results in the approximation (Ref. 38:125):

$$Q_r = \frac{kT}{\sigma hcB} \quad (41)$$

where the symmetry factor of CO_2 , $\sigma = 2$. Therefore, Q_r varies as the temperature, T . The U.S. Standard Atmosphere, 1976 (Ref. 39:53) was used for temperatures and pressures at various altitudes. Using the values for Q_v , E'' , and Equations (38) and (40), "off"-resonance cross sections for CO_2 as function of altitude are calculated. Then, to obtain an extinction coefficient as a function of altitude, it is necessary to multiply each cross section by the molecular number density of CO_2 at the corresponding altitude. The number density of CO_2 is assumed to be uniformly mixed at 330ppm of the total molecular density as a function of altitude (Ref. 23:6). Absorption cross sections, number densities, and extinction coefficients for "off"-resonance CO_2 can be found in Appendix H.

Extinction Coefficient of Carbon Monoxide

Calculation of extinction coefficients of carbon monoxide as a function of altitude closely parallels that of CO_2 above. However, a few differences exist. McClatchey (Ref. 10:4) reports that Q_v does not vary as temperature. Therefore, $Q_v(T_s)/Q_v(T) = 1$. Also, in Equation (40), $j = 1$ for CO. The energy of the lower transition state (E'') for a diatomic molecule can be approximated as (Ref. 51:V-2)

$$E''_{J,v} = B''J''(J'' + 1) + (v'' + \frac{1}{2})\overline{\omega}_e - \chi_e(v'' + \frac{1}{2})^2\overline{\omega}_e \quad (42)$$

where for CO as previously stated

$$B'' = 1.9225\text{cm}^{-1}$$

$$\overline{\omega}_e = 2169.74\text{cm}^{-1}$$

$$\chi_e = .0061$$

The lower vibrational energy state of the (1-0) band is ground state, so $v'' = 0$. The rotational line closest to "off"-resonance frequency is the P(19) line, so $J'' = 19$. Therefore, E'' has a value approximately equal to 1812.12cm^{-1} . From Equation (38), absorption cross sections as a function of altitude can be calculated. As previously stated CO is considered a uniformly mixed gas with a number density of .075ppm, so number densities at various altitudes can be calculated. Appendix I lists the cross sections, number densities, and extinction coefficients for CO as a function of altitude for the "off"-resonance frequency.

Extinction Coefficient of Ozone

These calculations are similar to those above.

McClatchey (Ref. 10:4) reports the following values for Q_v as a function of temperature:

<u>Temp(K)</u>	175	200	225	250	275	296
<u>$Q_v(T)$</u>	1.004	1.007	1.013	1.022	1.032	1.046

The ratio of the rotation partition functions is given by Equation (40), but for ozone, $j = 1.5$. Since the spectra of ozone is very complicated, with numerous lines contributing to absorption, E'' is taken as an average of the sum of the lower energy levels of the 170 evaluated lines. Flaud and Camy-Peyret (Ref. 37:192) provide values of E'' for each individual absorption line. Calculating the mean gives $E'' = 827.400\text{cm}^{-1}$. With these values, and Equation (38), cross sections as a function of altitude are calculated.

Ozone is not a uniformly mixed gas. However, U.S. Standard Atmosphere, 1976 provides number densities as a function of altitude for a mid-latitude ozone model (Ref. 39:38). Using these values along with the cross sections, extinction coefficients as a function of altitude can be calculated from Equation (17), which are found in Appendix J. In addition, the extinction coefficients were graphed versus altitude, and interpolation provided the additional values found in Appendix J.

It should be noted that the extinction coefficient of ozone does not vary a great deal with altitude due to a balancing of a decreasing cross section multiplied by an increasing number density, which is in direct contrast to CO and CO₂ extinction coefficients, which decrease rapidly with altitude. Therefore, a check to determine whether absorption above 30 kilometers is significant, where Doppler broadening is dominant, must be made. From Equation (36) the line intensity at 31 kilometers of the line contributing the most to absorption at the "off"-resonance frequency (2057.024cm⁻¹) is given by:

$$S(T) = S(T_s) \left[\frac{Q_v(T_s)}{Q_v(T)} \frac{Q_r(T_s)}{Q_r(T)} \right] \exp \left[\frac{1.439(T - T_s)E''}{TT_s} \right]$$

where

$$S(T_s) = 5.77 \times 10^{-23} \text{ cm}^{-1} \text{ cm}^2 \text{ mol}^{-1} \text{ (Appendix G)}$$

$$T = 227.5^\circ \text{K at 31 kilometers.}$$

$$\text{This gives } S(T) = 2.631 \times 10^{-23} \text{ cm}^{-1} \text{ cm}^2 \text{ mol}^{-1}$$

Equation (20) gives the Gaussian half-width as

$$\alpha_D = \frac{v_o}{c} \left((\ln 2) 2kT/m \right)^{\frac{1}{2}}$$

where for ozone

$$m = 48 \text{ amu } (1.6604 \times 10^{-24} \text{ gr/amu})$$

$$v_o = 2057.054 \text{ cm}^{-1} \text{ (Appendix G)}$$

$$\text{This gives } \alpha_D = 1.60 \times 10^{-3} \text{ cm}^{-1}.$$

The cross section is given by Equation (20):

$$\sigma(\lambda) = (S/\alpha_D)(\ln 2/\pi)^{\frac{1}{2}} \exp \left[-(\lambda - \lambda_0)^2 \ln 2 / \alpha_D^2 \right]$$

Substituting the above values gives $\sigma(\lambda) \approx 0$. Therefore, extinction above 30 kilometers can be neglected.

Extinction Coefficient of Water Vapor

These coefficients are calculated in the same manner as the ozone above with only minor differences. McClatchey (Ref. 10:4) reports that the vibrational partition function does not vary with temperature. Since H_2O has the same structure as ozone, the value of j in Equation (40) is also 1.5. Averaging over the 107 lower energy states provided by Flaud and Camy-Peyret (Ref. 36) gives a mean E'' of 1709.79 cm^{-1} . Using these values and Equation (38), absorption cross sections as a function of altitude are calculated.

The number density of water vapor is not uniformly mixed. Instead, it varies a great deal, depending on the atmospheric conditions. U.S. Standard Atmosphere, 1976 provides data for a mixing ratio of water vapor mass to dry air for an average mid-latitude model for various altitudes (Ref. 38:44). After converting this data to molecular number density by volume, extinction coefficients as a function of altitude can be computed using Equation (17), results are found in Appendix K.

Calculation of "Off"-Resonance Return Signal Power

The returned signal power for the "off"-resonance frequency is determined from the basic lidar equation, Equation (4):

$$P_{2j} = \frac{P_o EK A_r}{R_j^2} \left(\frac{\tau_c}{2} \right) s_{2j} \exp \left[-2 \int_0^{R_j} (\xi_2 + N_{CO_2} \sigma_2) dr \right] \quad (43)$$

where

$$P_o = 2 \text{ joules/100n sec}$$

$$EK = (.1)(.3) = .03$$

$$A_r = r^2 = 7.854 \times 10^{-7} \text{ km}^2$$

$$\frac{CT}{2} = R = 1 \text{ km}$$

To determine the returned power from various altitudes the exponential of Equation (43) must be evaluated. Since the extinction coefficients do not vary as simple functions of r , numerical integration is used where:

$$\int_0^{R_j} (\xi_2 + N_{CO_2} \sigma_2) dr \approx \sum_i < \xi_2 + N_{CO_2} \sigma_2 > \Delta r_i \quad (44)$$

where

$$\xi_2 = \xi_2^{O_3} + \xi_2^{H_2O} + \xi_{2R} + \xi_{2M}$$

$$\Delta r_i = 1 \text{ km}$$

where ξ_{2R} and ξ_{2M} = extinction coefficient due to Rayleigh and Mie scattering.

As an example, consider an evaluation of the return signal from a one-kilometer cell from four to five kilometers in altitude, or when $R_j = 196\text{km}$. For this example, Equation (44) takes the form of:

$$\int_{170}^{196} (\xi_2 + N_{\text{CO}_2} \sigma_2) dr \approx \sum_{i=170}^{196} \langle \xi_2^{\text{H}_2\text{O}} + \xi_2^{\text{CO}} + \xi_2^{\text{O}_3} + \xi_{2R} + \xi_{2M} + N_{\text{CO}_2} \sigma_2 \rangle \Delta r_i$$

where summations are done over extinction coefficients found in the applicable appendices. In this case,

$$\int_{170}^{196} (\xi_2 + N_{\text{CO}_2} \sigma_2) dr \approx .2924.$$

The only additional unknown term in Equation (43) is the total volumetric backscattering coefficients, which is the sum of the Rayleigh and Mie backscattering coefficients.

Equation (15) gives the expression for the Rayleigh backscattering coefficient as:

$$s_{ijR} = \frac{3}{8\pi} \xi_{iR}$$

The direction of Mie scattering depends heavily on particle size, but is only generally considered isotropic (Ref. 24:1502). Therefore, the backscattering coefficient due to Mie scattering is given by:

$$s_{ijM} = \frac{1}{4\pi} \xi_{iM} \quad (45)$$

Using the scattering coefficients from Appendices A and B at 196km, the total backscattering coefficients can be calculated from:

$$\beta_{2,j} = \frac{2.32 \times 10^{-4}}{4\pi} + \frac{1.28 \times 10^{-6}(3)}{8\pi} = 1.86 \times 10^{-5} \text{ km}^{-1} \text{ sr}^{-1}$$

Substituting these values into Equation (43), the returned signal power from scattering from an altitude of four to five kilometers ($R_j = 196$) is:

$$P_{2j} = 1.27 \times 10^{-10} \text{ Watts}$$

Similar calculations are done for $R_j = 190$ to 200. Results of the total backscattering coefficients and returned signal power at various altitudes are displayed in Table I.

Background Noise Calculations

Three basic sources of background exist:

1. Radiance from the earth.
2. Radiance from the sun.
3. Radiance from the sky.

Radiance from the earth is considered as blackbody radiance at a temperature of 296°K. The equation governing the amount of power in watts received at the lidar detector due to the earth's background radiance is (Ref. 20:25):

$$P_B^e = W(\lambda) \Delta\lambda \frac{\pi^2}{16} D^2 \theta^2 K T_a' \quad (46)$$

Table I

Backscattering Coefficient and Returned Power
at "Off"-Resonance Frequency

R_j (km)	β_{2j} ($\text{km}^{-1} \text{sr}^{-1}$)	P_{2j} (W)
190	2.520×10^{-6}	3.225×10^{-11}
191	1.655×10^{-6}	2.068×10^{-11}
192	2.867×10^{-6}	3.457×10^{-11}
193	5.195×10^{-6}	5.918×10^{-11}
194	7.516×10^{-6}	7.793×10^{-11}
195	1.120×10^{-5}	9.935×10^{-11}
196	1.861×10^{-5}	1.271×10^{-10}
197	3.717×10^{-5}	1.580×10^{-10}
198	3.082×10^{-4}	5.932×10^{-10}
199	5.135×10^{-4}	2.876×10^{-10}
200	7.960×10^{-4}	3.986×10^{-11}

where

$W(\lambda)$ = Spectral radiance of the earth

$(Wcm^{-2}\mu^{-1}sr^{-1})$

$\Delta\lambda$ = Spectral band width (μ)

D = Diameter of receiver telescope (cm)

θ = Field of view of the telescope (assumed
conical with θ full cone angle)

K = Transmittance of receiver optics

T'_a = Atmospheric transmittance

For operation on the "off"-resonance frequency, T'_a can
be determined from:

$$T'_a = \exp \left\{ - \int_0^{200} (\xi_2 + N_{CO_2} \sigma_2) dr \right\} \quad (47)$$

Extinction coefficients are found in Appendices A, B, and H-K.

In this case $T'_a = 6.52 \times 10^{-2}$. Also, K is again

taken as .3. To minimize background, θ and λ should be
minimized. θ is selected to minimize the background

signal from the target, while at the same time ensuring that
the FOV encompasses the laser spot size at the target. θ

is assumed to be 10^{-4} radians (Ref. 20:28), which gives a

spot size on the earth of diameter, $d = \theta R_j = 200 \times$

$10^3(10^{-4}) = 20m$. If the transmitted laser beam is

designed to also have a spot size of diameter, $d = 20m$, then

the spot size (radius) leaving the shuttle is given for a

far-field approximation by (Ref. 49:4-13):

$$w_o \approx \frac{\lambda R_j}{\pi w(z)}$$

where

$w(z)$ = Spot size at range R_j (m)

Substituting applicable values gives $w_o \approx 3.09$ cm, a reasonable value for this system.

The width of a CO_2 absorption line, $\Delta\lambda$, averages $.07 \text{ cm}^{-1}$, or since $\lambda = \frac{1}{\nu}$, $\Delta\lambda = 1.65 \times 10^{-4} \mu$.

For this study a spectral bandwidth, $\Delta\lambda = 6.75 \times 10^{-3} \mu$, was selected based on available filters at about 5μ . The radiance of the earth is given by:

$$L_e = W(\lambda) \Delta\lambda$$

Since the earth radiates as a nearly perfect blackbody at $\lambda = 4-5\mu$ the radiance can be determined from (Ref. 41:24):

$$L_e = \frac{e M_{e\lambda_1 \rightarrow \lambda_2}}{\pi} \quad (49)$$

where

$$\begin{aligned} M_{e\lambda_1 \rightarrow \lambda_2} & \text{ (emittance in spectral window of} \\ & \text{a perfect blackbody)} \\ &= \int_0^{\lambda_2} M_e(\lambda) d\lambda - \int_0^{\lambda_1} M_e(\lambda) d\lambda \end{aligned} \quad (50)$$

e (Emissivity) = .85 (Ref. 29:3-90).

Radiation tables (Ref. 40) provide ratios of the emittance of a blackbody. The total emittance is given by the Stefan-Boltzmann Law:

$$M_e = \sigma T^4 \quad (51)$$

where

$$\sigma = 5.672 \times 10^{-8} \text{ Wm}^{-2} \text{ } ^\circ\text{K}^{-4}$$

To get $\Delta\lambda = 6.757 \times 10^{-3} \mu$, the minimum and maximum wavelengths used were $\lambda_1 = 4.858108 \mu$ and $\lambda_2 = 4.864865 \mu$. Using Equations (49), (50), and (51), $L_e = 5.749 \times 10^{-7} \text{ Wcm}^{-2} \text{ sr}^{-1}$. Substituting appropriate values into Equation (46), gives $P_B^e = 8.17 \times 10^{-13} \text{ W}$.

Calculation of background due to the sun's radiation is very similar. The power received is given by:

$$P_B^{\text{sun}} = W(\lambda) \lambda \frac{\pi^2}{16} D^2 \theta^2 T_a'^2 r K \quad (52)$$

where

r = reflectivity of earth at 4.86μ estimated at .15
(Ref. 29:3-90)

Atmospheric transmittance is squared since radiation must pass through the atmosphere twice. The sun is also considered a blackbody, but at a temperature of 5900°K . The radiance, L_e , is calculated using radiation tables in a similar manner to that described above. L_e is

calculated as $\frac{1.00}{4.57} \times 10^{-6} \text{ Wcm}^{-2} \text{ sr}^{-1}$. From Equation (52), the background noise due to the reflected sun's radiance is calculated as $p_B^{\text{sun}} = \frac{3.95}{1.79} \times 10^{-8} \text{ W}$.

Background noise as a result of sky radiance is more difficult to analyze. This background is a result of scattering of the sun's radiance and emission by atmospheric constituents. However, essentially the scattering occurs below 3μ and the thermal emission above 4μ (Ref. 29:3-71). To account for this additional background the experimental data by Bell (Ref. 42:1318) has been used. Bell estimates the sky spectral radiance at 4.86μ as $2.13 \times 10^{-4} \text{ Wcm}^{-2} \mu^{-1} \text{ sr}^{-1}$. Multiplying by $\Delta\lambda$ gives a radiance, $L_e = 1.439 \times 10^{-6} \text{ Wcm}^{-2} \text{ sr}^{-1}$. Losses due to additional atmospheric scattering are ignored so the background due to sky radiance received at the detector is given by:

$$p_B^{\text{sky}} = L_e \frac{\pi^2}{16} D^2 \Theta^2 K \quad (53)$$

$$p_B^{\text{sky}} = 2.66 \times 10^{-11} \text{ W}.$$

The total background is the sum of the three individual background noises:

$$P_B = p_B^e + p_B^{\text{sun}} + p_B^{\text{sky}} \quad (54)$$

$$P_B = \frac{2.78}{1.79} \times 10^{-11} \text{ W}$$

Signal-to-Noise Calculations (Direct Detection)

The detector offering the most efficient normalized detectivity in the 4.86μ region is the indium antimonide (InSb) photovoltaic infrared detector operating at 77°K . Kildal and Byer state that a photovoltaic InSb detector is always dark-current limited for normal bandwidths. In this case they give the normalized detectivity as (Ref. 43:1648):

$$D^* = \frac{S_D}{\sqrt{2e(i_d/A_D)}} \quad (55)$$

or by rewriting, the dark current is given as:

$$i_d = \frac{S_D^2 A_D}{2eD^{*2}} \quad (56)$$

where for a Ford Aerospace and Communications InSb infrared detector (ISC-386 series)

$$S_D \text{ (Sensitivity of the detector)} = 2.0^{\text{A}}/\text{W}$$

$$e = 1.602 \times 10^{-19} \text{C}$$

$$D^* = 8.6 \times 10^{10} \text{ cm Hz}^{\frac{1}{2}} \text{ W}^{-1} \text{ for a } \theta_{\frac{1}{2}} = 60^\circ$$

However, the field of view developed earlier has $\theta_{\frac{1}{2}} = 5 \times 10^{-5} \text{ rad}$. Therefore, it is necessary to develop a new normalized detectivity from the equation below (Ref. 44:45):

$$D^{**} = D^* \sin \theta_{\frac{1}{2}}$$

$$D^{**} = 7.45 \times 10^{10} \text{ cm Hz}^{\frac{1}{2}} \text{ sr}^{\frac{1}{2}} \text{ W}^{-1}.$$

Therefore, for a FOV of 10^{-4} rad , $D^* = 1.49 \times 10^{15} \text{ cm Hz}^{\frac{1}{2}} \text{ W}^{-1}$.

Substituting into Equation (56) $i_d = 1.59 \times 10^{-14} \text{ A}$.

However, the current due to the returned laser signal is approximately:

$$\begin{aligned} i_s &= P_s S_D & (58) \\ i_s &= (1.27 \times 10^{-10})(2.0) \text{ at } R_j = 196 \text{ km} \\ i_s &= 2.54 \times 10^{-10} \text{ A} \end{aligned}$$

Therefore, since the FOV is so narrow, the InSb detector cannot be considered dark current limited, and i_d can be neglected in future calculations.

The power signal-to-noise ratio for photovoltaic photodiode is given by (Ref. 41:169):

$$\left(\frac{S}{N}\right)_i = \left[\frac{\overline{i_s^2}}{\overline{i_{N_1}^2} + \overline{i_{N_2}^2}} \right]^{\frac{1}{2}} = \left[\frac{2m^2 \frac{P_{ij}\eta e^2}{hf}}{\left[\frac{2e^2\eta\Delta f}{hf} \left\{ \left(1+\frac{m^2}{2}\right) P_{ij} + \left(1+\frac{m^2}{2}\right) P_B \right\} + 2e i_d \Delta f + \frac{4kT_e \Delta f}{R_L} \right]} \right]^{\frac{1}{2}} \quad (59)$$

where

$$\overline{i_s^2} = 2m^2 \left(\frac{P_{ij}\eta e}{hf} \right)^2 \quad (\text{mean-square current due to the return signal})$$

$$\overline{i_{N_1}^2} = 2e\Delta f \left[\left(1+\frac{m^2}{2}\right) \frac{P_{ij}\eta e}{hf} + \left(1+\frac{m^2}{2}\right) \frac{P_B\eta e}{hf} + i_d \right]$$

(mean-square current due to shot noises of the

returned signal, background, and dark current)

$$\overline{i_{N_1}^2} = \frac{4kT_e \Delta f}{R_L} \quad (\text{Johnson or thermal noise due to the detector, load resistor, and amplifier})$$

η = Detector quantum efficiency

f = frequency of operation corresponding to "on"
or "off" resonance (Hz)

Δf = electrical bandwidth of the detection system (Hz)

m = Order of the modulated optical beam.

T_e = Effective temperature of the load resistor,
including amplifier noise.

R_L = Load resistor of the detection system ($R_L \ll R_d$)

For an "off"-resonance pulse, $f = 6.1668 \times 10^{13}$ Hz,
 η is taken as a conservative .3 (Ref. 20:264), and $m = 1$.
The electrical bandwidth must be large enough that it is
responsive to the return laser signal. Commonly, the
minimum bandwidth is taken as:

$$\Delta f = \frac{1}{2\tau}$$

where

$$\tau (\text{intergration time of the returned power signal}) = \frac{2\Delta R}{c} = 6.67 \times 10^{-6} \text{ sec}$$

In this case, $\Delta f = 7.495 \times 10^4$ Hz.

The effective temperature (T_e) includes the
effective noise temperature of the amplifier, T_A . T_A is
determined from the amplifier noise figure, F , where
(Ref. 41:169):

$$F = 1 + \frac{T_A}{290}$$

If F has a realistic value of 2 (Ref. 41:170), then $T_A = 290^\circ\text{K}$. The effective temperature, T_e , is the sum of the detection system temperature plus the amplifier temperature:

$$T_e = T + T_A$$

If $T = 290^\circ\text{K}$, then $T_e = 580^\circ\text{K}$.

Typically, for a photodiode the load resistor is selected to be less than the impedance of the detector, R_d , which for ISC-386 series photodiode is 25×10^3 ohms, and much greater than the spread resistance, R_s , typically 50 ohms. For this study, $R_L = 1000$ ohms.

As an example, the signal-to-noise ratio for a return signal from $R_j = 196\text{km}$ is given by:

$$\left(\frac{S}{N}\right)_2 = \left[\frac{4.470 \times 10^{-20}}{7.638 \times 10^{-22} + 2.400 \times 10^{-18}} \right]^{\frac{1}{2}} = .136$$

As can be seen, $(S/N)_2$ does not meet the minimum requirement of $(S/N)^2 = 2$ as given in Equation (12). Clearly, the dominating noise (second term in the denominator) is the Johnson or thermal noise of the detector, load resistor, and amplifier. Unfortunately, there is little that can be done to reduce the thermal noise the two orders of magnitude necessary to achieve an acceptable $(S/N)_2$.

Heterodyne Detection

The best alternative to achieve an acceptable $(S/N)_2$ without changing any of the given parameters of

the study is by coherent or heterodyne detection, where the incoming wave's amplitude and phase are converted to a low frequency in the rf or microwave region. Heterodyne detection was initially proposed for IR or visible frequency signals in the 1960's, and has since successfully demonstrated on numerous occasions including recent experiments with pulsed CO₂ lidars by Cruickshank (Ref. 45:290) and Lundquist (Ref. 46:2534).

To obtain this low frequency signal, the incoming signal is mixed with that of a continuous beam of slightly different frequency from a local oscillator (See Figure 4). The effects of this mixing are discussed below for the simple case of equal phase, constant amplitude co-planar waves (Ref. 47:24). The total electric field, E , of the incident waves is given by:

$$E = E_{LO} \cos \omega_{LO} t + E_{ij} \cos \omega_{ij} t \quad (61)$$

where

E_{LO} = Electric field of the local oscillator with frequency, ω_{LO} .

E_{ij} = Electric field of the returned signal at frequency, ω_{ij} .

The photodetector current from the combined signal is given by:

$$i(t) = \frac{e \eta P(t)}{h f} \quad (62)$$

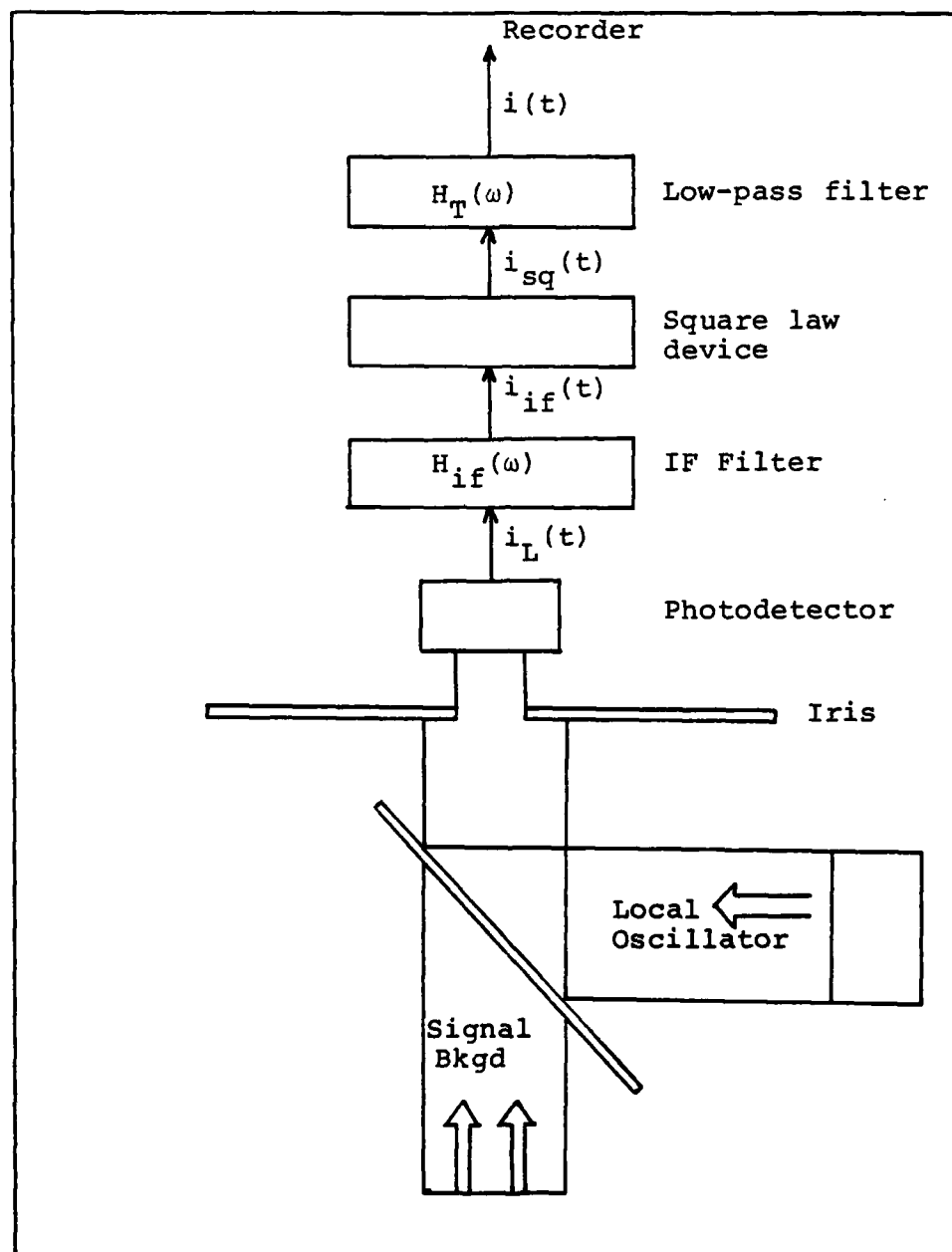


Figure 4: Block Diagram of a Laser Radar
With Heterodyne System (Ref. 48:258)

The power can also be expressed as:

$$P(t) = \frac{E^2(t)A_d}{z_o} \quad (63)$$

where

A_d = Detector area

z_o = Impedance of free space

Combining Equations (61), (62), and (63):

$$i(t) = \frac{e\eta A_d}{z_o hf} \left[\frac{1}{2} E_{LO}^2 (1 + \cos 2 \omega_{LO} t) + \frac{1}{2} E_{ij}^2 (1 + \cos 2 \omega_{ij} t) + E_{LO} E_{ij} \cos(\omega_{ij} - \omega_{LO})t + E_{LO} E_{ij} \cos(\omega_{ij} + \omega_{LO})t \right] \quad (64)$$

The final term can be ignored since the electronics will not resolve the combined frequencies. Recalling the $i_{LO} =$

$\frac{e\eta A_d}{2z_o hf} E_{LO}^2$ and $i_{ij} = \frac{e\eta A_d}{2z_o hf} E_{ij}^2$ gives:

$$i(t) = i_{LO} + i_{ij} + 2 \sqrt{i_{LO} i_{ij}} \cos(\omega_{ij} - \omega_{LO})t \quad (65)$$

To calculate the power $(S/N)_i$ due to the intermediate frequency (i.f.) current, take the mean-square i.f. current:

$$\overline{i_{if}^2} = (2 \sqrt{i_{LO} i_{ij}})^2 / 2 = 2 i_{LO} i_{ij} \quad (66)$$

If the shot noise is dominated by the local oscillator beam, by design, then the mean-square shot noise current for a photodiode is given by (Ref. 47:25):

$$\overline{i_N^2} = 4e i_{LO} B_{if} \quad (67)$$

where

B_{if} = Bandwidth of the i.f. channel following the
detector (Hz)

Including the thermal noise of the detection system gives
the power signal-to-noise ratio as (Ref. 47:41):

$$\left(\frac{S}{N}\right)_i = \frac{i_{if}^2}{i_N^2 + \frac{4kT_e B_{if}}{R_L}} \quad (68)$$

Combining Equations (66), (67), and (68) gives

$$\left(\frac{S}{N}\right)_i = \frac{\eta P_{ij}}{hfB_{if} \left(2 + \frac{2kT_e hf}{e^2 P_{LO} R_L} \right)} \quad (69)$$

In order to ensure that the shot noise of the local
oscillator dominates the thermal noise of the detection
system:

$$P_{LO} \gg \frac{2kT_e hf}{e^2 \eta R_L} \quad (70)$$

Assuming the same values for the variables as previously
given, the local oscillator power must be greater than $4.249 \times 10^{-5} W$. A reasonable value would be .1W, accounting for
the required frequency-doubling crystal. If a local
oscillator is used then the power signal-to-noise ratio is
given by:

$$\left(\frac{S}{N}\right)_i = \frac{\eta P_{ij}}{2hfB_{if}} \quad (71)$$

Several important features can be summarized at this time
(Ref. 47:26):

1. The i.f. signal power is proportional to the returned signal, P_{ij} .
2. $\left(\frac{S}{N}\right)_i$ is inversely proportional to the bandwidth.
3. The output i.f. spectrum for a broad-band signal is an exact replica of the input optical spectral distribution, provided the local oscillator is a single-frequency wave with nonfluctuating phase.

Table II lists values for $\left(\frac{S}{N}\right)_2$ for values of P_{2j} with values of $j = 190$ to 200km , assuming $B_{ij} = \Delta f$. Equation (71) gives the common equation for $\left(\frac{S}{N}\right)_i$. However, two problems exist with this analysis. First, it does not account for random signal fluctuation, and second, the coherence of the signal may not be maintained during its analysis. In a pulsed signal, the coherence, at best, is usually the pulse length. If $B_{if}t' < 1$, then a temporal averaging factor must be added. A more accurate expression of $\left(\frac{S}{N}\right)_i$ has been developed by Elbaum (Ref. 48:257):

$$\left(\frac{S}{N}\right)_{Hi} = \frac{\langle i(t) \rangle - \langle i(t) \rangle_0}{\left[\text{Var } \{i(t)\} \right]^{\frac{1}{2}}} \quad (72)$$

Table II

Ideal $\left(\frac{S}{N}\right)_2$ for Heterodyne Detection ($B_{if} = 7.945 \times 10^4 \text{ Hz}$)

$R_j \text{ (km)}$	$\left(\frac{S}{N}\right)_2$
190	1.58×10^3
191	1.01×10^3
192	1.69×10^3
193	2.90×10^3
194	3.82×10^3
195	4.87×10^3
196	6.23×10^3
197	7.74×10^3
198	2.91×10^4
199	1.36×10^4
200	1.95×10^3

where

$\langle i(t) \rangle$ and $\langle i(t)_o \rangle$ = average values of output current in the presence and absence of signal, respectively.

For a photodiode, this takes the form of (Ref. 22:1175):

$$\left(\frac{S}{N}\right)_{Hi} = \frac{P_{ij} \cdot \left[(2^{\Delta R/c}) (B_{if}) \right]^{\frac{1}{2}}}{\left\{ \frac{hf}{\eta} \left(1 + \frac{P_B}{P_{LO}} \right) + \frac{k(T+T_a)}{G} \right\} B_{if} + P_{ij}} \quad (73)$$

where

$$G(\text{heterodyne conversion gain}) = \frac{P_{LO}}{2G_D} \left(\frac{\eta e}{hf} \right)^2 \frac{1}{1 + (f/f_e)^2} \quad (74)$$

where

G_D = Incremental shunt conductance.

f_e = Rolloff frequency of the photodiode.

If P_{LO} shot noise again is designed to dominate other noise forms, then Equation (73) becomes:

$$\left(\frac{S}{N}\right)_{Hi} = \frac{P_{ij} \left[(2^{\Delta R/c}) (B_{if}) \right]^{\frac{1}{2}}}{\frac{hf}{\eta} B_{if} + P_{ij}} \quad (75)$$

Note, that the term $\left[(2^{\Delta R/c}) (B_{if}) \right]^{\frac{1}{2}}$ must be at least four if P_{ij} is the dominate term in the denominator, and $\left(\frac{S}{N}\right)_{Hi}$ is to be greater than two. Therefore, select $B_{if} = 10^7 \text{ Hz}$.

Table III lists values of $\left(\frac{S}{N}\right)_{H2}$ for $R_j = 190-200 \text{ km}$ with $B_{ij} = 10^7 \text{ Hz}$. Note that all values exceed the minimum $\left(\frac{S}{N}\right)_2$ requirement of two given in Equation (12).

Table III

Actual $\left(\frac{S}{N}\right)_{H2}$ for Heterodyne Detection ($B_{if} = 10^7 \text{ Hz}$)

$R_j \text{ (km)}$	$\left(\frac{S}{N}\right)_{H2}$
190	7.84
191	7.66
192	7.86
193	7.98
194	8.03
195	8.06
196	8.08
197	8.10
198	8.15
199	8.13
200	7.902

Detection of Hot CO₂ in the Atmosphere

It is conceivable that shuttle observations could detect CO₂ hot spots in the atmosphere due to a high energy laser facility or fossil fuel-burning plant. Equation (4) gives the basic DIAL equation for the return power from a shuttle lidar. If a quantity of hot CO₂ gas is introduced into the atmosphere then the basic equation is altered to:

$$P'_{ij} = \frac{EP_o K A_r}{R_j^2} \left(\frac{c\tau}{2} \right) s_{ij} \exp \left\{ -2 \int_0^{R_j} (\xi_i + CO_2 \sigma_i + N_{CO_2}^H \sigma_i^H) dr \right\} \quad (76)$$

where

$$\begin{aligned} N_{CO_2}^H &= \text{Number density of hot CO}_2 \text{ molecules.} \\ \sigma_i^H &= \text{Absorption cross section for CO}_2 \text{ at a given} \\ &\quad \text{temperature, T.} \end{aligned}$$

This analysis will determine the maximum number density of hot CO₂, $N_{CO_2}^H$, that can be detected, and still meet the minimum $\left(\frac{S}{N} \right)_i$ requirement of two as stated in Equation (12). The minimum "off"-resonance power is determined from Equation (74):

$$\begin{aligned} \left(\frac{S}{N} \right)_{H2} = 2 &= \frac{P_{2j} \left[\left(2 \frac{\Delta R}{c} \right) (B_{2f}) \right]^{\frac{1}{2}}}{\left(\frac{hf B_{2f}}{\eta} \right) + P_{2j}} \\ P_{2j \text{ min}} &= \frac{2hf B_{2f}}{\eta \left\{ \left[\left(2 \frac{\Delta R}{c} \right) (B_{2f}) \right]^{\frac{1}{2}} - 2 \right\}} \\ P_{2j \text{ min}} &= 4.42 \times 10^{-13} W \end{aligned}$$

In order to determine the number density of the hot CO_2 that will give that minimum return power, it is necessary to determine the absorption cross sections at various high temperatures. Equation (38) gives the "off"-resonance absorption for CO_2 as function of pressure and temperature:

$$\sigma_{2\text{CO}_2}^{\text{H}}(P, T) = \sigma_{2\text{CO}_2} \left[\frac{Q_v(T_s)}{Q_v(T)} \frac{Q_r(T_s)}{Q_r(T)} \right] \exp \left[\frac{1.439(T-T_s)E''}{TT_s} \right] \left[\frac{P}{P_s} \right] \left[\frac{T_s}{T} \right]^{\frac{1}{2}}$$

where $\sigma_{2\text{CO}_2} = 1.361 \times 10^{-21} \text{ cm}^2$, and $E'' = 2447.23 \text{ cm}^{-1}$.

Unfortunately, McClatchey does not provide values for the vibrational partition function, Q_v , for temperatures over 296°K . Therefore, it is necessary to compute values. As previously stated the vibrational partition function is given by:

$$Q_v = \sum_{v_1, v_2, v_3, l} g_l \exp \left[- \frac{E_v}{kT} \right]$$

A good approximation is the harmonic oscillator approximation, which assumes the energy levels are integer multiples of the fundamental frequencies. This, along with the identity $\sum_{v_i=0}^{\infty} \exp \left\{ -E_i v_i / kT \right\} = (1 - \exp \left\{ -E_i / kT \right\})^{-1}$,

gives the harmonic approximation of the vibrational partition function (Ref. 38:52):

$$Q_v = \left(\frac{1}{1 - e^{-E_1/kT}} \right) \left(\frac{1}{1 - e^{-E_2/kT}} \right)^2 \left(\frac{1}{1 - e^{-E_3/kT}} \right) \quad (77)$$

where

$$E_1/k = 1.439\bar{\nu}_1$$

$$\bar{\nu}_1 = 1330.0\text{cm}^{-1}$$

$$E_2/k = 1.439\bar{\nu}_2$$

$$\bar{\nu}_2 = 667.3\text{cm}^{-1}$$

$$E_3/k = 1.439\bar{\nu}_3$$

$$\bar{\nu}_3 = 2349.3\text{cm}^{-1}$$

Therefore, the ratio of the vibrational partition function is given by:

$$\frac{Q_v(T_s)}{Q_v(T)} = \frac{(1 - e^{-1.439\bar{\nu}_1/T})(1 - e^{-1.439\bar{\nu}_2/T})^2 (1 - e^{-1.439\bar{\nu}_3/T})}{(1 - e^{-1.439\bar{\nu}_1/T_s})(1 - e^{-1.439\bar{\nu}_2/T_s})^2 (1 - e^{-1.439\bar{\nu}_3/T_s})} \quad (78)$$

The ratio of the rotational partition functions is again given by Equation (40):

$$\frac{Q_r(T_s)}{Q_r(T)} = \left(\frac{T_s}{T} \right)^j$$

where $j = 1$ for CO_2 .

Four assumptions are made in this analysis:

1. The additional hot CO_2 does not significantly add to the atmospheric pressure as a function of altitude.
2. The gas has diffused and cooled above 2 kilometers.

3. The laser illuminates a uniform area of hot CO_2 .
4. The hot CO_2 occupies only a single one-kilometer cell, and N_{CO_2} , and σ_{HCO_2} are constant over the cell.

With these assumptions, and pressure data from the U.S. Standard Atmosphere, 1976, "off"-resonance absorption cross sections can be calculated for temperatures from $T = 400^\circ\text{K}$ - 1000°K . Appendix L lists these values for altitudes from 0-2 kilometers.

By combining the basic DIAL equation, Equation (4), and the modified DIAL equation that accounts for the hot CO_2 , Equation (76), relationship between the returned signals can be expressed as:

$$P'_{2j} = P_{2j} \exp \left\{ -2 \int_0^{R_j} N_{\text{CO}_2}^{\text{H}} \sigma_{2\text{CO}_2}^{\text{H}} dr \right\} \quad (79)$$

The minimum acceptable returned power, $P_{2j \text{ min}}$, is substituted for P'_{2j} to get the maximum $N_{\text{CO}_2}^{\text{H}}$. Values for P_{2j} are found in Table II. Therefore, for $R_{2j} = 198\text{-}200\text{km}$, the integrated optical thickness of hot CO_2 is given as:

$$\int_0^{198} N_{\text{CO}_2}^{\text{H}} \sigma_{2\text{CO}_2}^{\text{H}} dr = 3.601$$

$$\int_0^{199} N_{\text{CO}_2}^{\text{H}} \sigma_{2\text{CO}_2}^{\text{H}} dr = 3.223$$

$$\int_0^{200} N_{\text{CO}_2}^{\text{H}} \sigma_{2\text{CO}_2}^{\text{H}} dr = 2.251$$

By using a one kilometer cell, and assuming constant density cross section over the cell, as stated in assumptions (3) and (4), the maximum hot CO₂ density can be computed. Results as a function of temperature for $R_j = 198-200$ are found in Table IV.

Table IV
Maximum Hot CO₂ Concentration for $\left(\frac{S}{N}\right)_{H_2} = 2$

Temp (°K)	$\sigma_{2CO_2}^H (cm^2)$	$N_{CO_2}^H (cm^{-3})$
$R_j = 198km$		
400	1.334×10^{-20}	2.70×10^{15}
500	4.824×10^{-20}	7.46×10^{15}
600	1.017×10^{-19}	3.54×10^{14}
700	1.581×10^{-19}	2.28×10^{14}
800	2.055×10^{-19}	1.75×10^{14}
900	2.382×10^{-19}	1.51×10^{14}
1000	2.546×10^{-19}	1.41×10^{14}
$R_j = 199km$		
400	1.507×10^{-20}	2.14×10^{15}
500	5.541×10^{-19}	5.91×10^{14}
600	1.149×10^{-19}	2.18×10^{14}
700	1.787×10^{-19}	1.80×10^{14}
800	2.322×10^{-19}	1.38×10^{14}
900	2.692×10^{-19}	1.20×10^{14}
1000	2.876×10^{-19}	1.12×10^{14}
$R_j = 200km$		
400	1.699×10^{-20}	1.32×10^{15}
500	6.145×10^{-20}	3.66×10^{14}
600	1.295×10^{-19}	1.74×10^{14}
700	2.015×10^{-19}	1.12×10^{14}
800	2.617×10^{-19}	8.60×10^{13}
900	3.035×10^{-19}	7.42×10^{13}
1000	3.243×10^{-19}	6.94×10^{13}

V. Error Analysis of DIAL Calculations

Equation (4) gives the returned signal power for a range-resolved DIAL system:

$$P_{ij} = \frac{EP_o K A_r}{R_j^2} \left(\frac{c\tau}{2} \right) s_{ij} \exp \left\{ -2 \int_0^{R_j} (\xi_i + N_{CO_2} \sigma_i) dr \right\}$$

When $i = 1$ designates the "on"-resonance frequency, $i = 2$ designates the "off"-resonance frequency, $j = 1$ designates a range cell, and $j = 2$ designates the $j + 1$ range cell, four equations of the basic DIAL equation can be expressed. Manipulation of these equations gives the expression for the optical thickness for a range cell R_1 to R_2 :

$$\int_{R_1}^{R_2} N_{CO_2} \Delta \sigma dr = \frac{1}{2} \left[\ln \frac{P_{11} P_{22}}{P_{12} P_{21}} - \ln \frac{s_{12} s_{21}}{s_{11} s_{22}} - 2 \int_{R_1}^{R_2} (\xi_1 - \xi_2) dr \right] \quad (80)$$

where

$$\Delta \sigma = \sigma_1 - \sigma_2$$

Since the volumetric backscattering coefficient varies slowly in infrared as a function of frequency, it can be assumed that $s_{12} \approx s_{21}$ when $\lambda_1 \approx \lambda_2$. Therefore, the second term of Equation (80) can be neglected. Also, Korb in his analysis selected his "on" and "off"-frequencies based on the analysis that extinction coefficients for other than CO_2 were equal for the two frequencies. For that reason, the third term of Equation (80) can be neglected.

Finally, if it is assumed the number density and cross section are constant over the range cell, then the number density can be expressed as:

$$N_{CO_2} = \left(\frac{1}{2\Delta\sigma\Delta R} \right) \ln \frac{P_{11}P_{22}}{P_{12}P_{21}} \quad (81)$$

Range-resolved differential absorption lidar data reduction involves the comparison of large amplitudes having small differences. The error of the CO_2 concentration depends heavily on errors in determining the magnitude of the returned signals. Errors can arise from laser wavelength, background noise, aerosol concentration, accuracy of H_2O vapor profile, lidar calibration procedures, and transmissivity due to atmospheric constituents. Because of these uncertainties it is not adequate to describe DIAL measurement accuracy based solely on $\left(\frac{S}{N} \right)_{Hi}$, but an expression must be developed that includes the random coherent noise within the signal (Ref. 21:557).

The error propagation by least squares (variance) for a function $f(x_1, \dots, x_n)$ is given by the expression (Ref. 19:8):

$$\left[\delta f(x_1, \dots, x_n) \right]^2 = \sum_{i=1}^n \left[\left(\frac{\delta f}{\delta x_i} \right)^2 (\delta x_i)^2 \right] \quad (82)$$

where

$$\left(\delta f(x_1 \dots x_n) \right)^2 = \frac{\sum_{j=1}^N \left[f(x_1^j \dots x_n^j) - f_0(x_{01}^j \dots x_{0n}^j) \right]^2}{N-1}$$

$$\delta x_i = \sqrt{\frac{\sum_{j=1}^N \left[x_i^j - x_{0i}^j \right]^2}{(N-1)}}$$

where the zero subscript denotes the mean value. For the case of determining the standard deviation of the CO₂ number density, Equation (81) reduces to:

$$\delta N = \left[N_{CO_2}^2 \left(\frac{\delta \Delta \sigma^2}{\Delta \sigma^2} + \frac{\delta \Delta R^2}{\Delta R^2} \right) + \left(\frac{1}{2 \Delta \sigma \Delta R} \right)^2 \sum_{i=1}^2 \sum_{j=1}^2 \frac{\delta P_{ij}^2}{P_{ij}^2} \right]^{\frac{1}{2}} \quad (83)$$

If it is assumed that the absorption cross section can be accurately verified through laboratory experimentation, and that the range cell height can be accurately determined from data analysis, then the standard deviation reduces to:

$$\delta N = \left[\left(\frac{1}{2 \Delta \sigma \Delta R} \right)^2 \sum_{i=1}^2 \sum_{j=1}^2 \frac{\delta P_{ij}^2}{P_{ij}^2} \right]^{\frac{1}{2}} \quad (84)$$

But P_{ij} cannot be directly measured. Instead P_{ij} can be expressed as:

$$P_{ij} = \frac{1}{Q} \left[\langle i(t) \rangle_{ij} - \langle i(t)_0 \rangle \right] \quad (85)$$

where

Q = Amplification factor (A/W).

$\langle i(t) \rangle$ and $\langle i(t)_o \rangle$ = Average values of the output current in the presence and absence of signal as stated in Equation (72).

Therefore, the variance of P_{ij} can be expressed as:

$$(\delta P_{ij})^2 = \frac{1}{Q^2} \left[\delta \langle i(t) \rangle_{ij}^2 - \delta \langle i(t)_o \rangle^2 \right] \quad (86)$$

Combining with Equations (84) and (85) gives:

$$\delta_N = \left[\left(\frac{1}{2 \Delta \sigma \Delta R} \right)^2 \sum_{i=1}^2 \sum_{j=1}^2 \frac{\delta \langle i(t) \rangle_{ij}^2 - \delta \langle i(t)_o \rangle^2}{(\langle i(t) \rangle_{ij} - \langle i(t)_o \rangle)^2} \right]^{\frac{1}{2}} \quad (87)$$

But from Equation (72), the heterodyne signal-to-noise ratio is given by:

$$\left(\frac{S}{N} \right)_{Hi} = \frac{\langle i(t) \rangle_i - \langle i(t)_o \rangle}{[\text{Var} \{ i(t) \}_i]^{\frac{1}{2}}}$$

Combining with Equation (87) gives:

$$\delta_N = \left[\left(\frac{1}{2 \Delta \sigma \Delta R} \right)^2 \sum_{i=1}^2 \sum_{j=1}^2 \left(\frac{1}{\left(\frac{S}{N} \right)_{Hi j}^2} - \frac{\delta \langle i(t)_o \rangle^2}{(\langle i(t) \rangle_{ij} - \langle i(t)_o \rangle)^2} \right) \right]^{\frac{1}{2}} \quad (88)$$

If the local oscillator results in the largest noise term, the variance of the background can be made very small, and the standard deviation of the number density can be approximated as:

$$\delta_N = \left[\left(\frac{1}{2 \Delta \sigma \Delta R} \right)^2 \sum_{i=1}^2 \sum_{j=1}^2 \left(\frac{1}{\left(\frac{S}{N} \right)_{Hi j}^2} \right) \right]^{\frac{1}{2}} \quad (89)$$

This is the expression for one pair of pulses ("on" and "off"-resonance). However, if signal of n pulse-pairs

are measured, then Equation (89) has the final form of
(Ref. 21:558):

$$\delta_N = \left[\left(\frac{1}{2 \Delta \sigma \Delta R} \right)^2 \frac{1}{n} \sum_{i=1}^2 \sum_{j=1}^2 \left(\frac{1}{\left(\frac{S}{N} \right)_{Hij}^2} \right) \right]^{\frac{1}{2}} \quad (90)$$

The number of pulse-pairs is related to the desired horizontal resolution. For CO₂ studies the NASA Working Group suggested $x = 100\text{km}$ (Ref. 7:18). If the shuttle velocity is 8km/sec (Ref. 15:626) with a laser repetition rate of 10Hz (Ref. 22:1181), then $n = 125$ shots.

The heterodyne signal-to-noise ratio was given in Equation (74) as:

$$\left(\frac{S}{N} \right)_{Hij} = \frac{P_{ij} \left[\left(\frac{2 \Delta R}{c} \right) B_{if} \right]^{\frac{1}{2}}}{\frac{hf B_{if}}{\eta} + P_{ij}}$$

This can be expressed as:

$$\left(\frac{S}{N} \right)_{Hij}^2 \approx \frac{P_{ij}}{P_N}$$

where P_N (quantum noise-equivalent power) = $\frac{hf}{\eta} (B_{if} \frac{c}{2 \Delta R})^{\frac{1}{2}}$

Therefore, Equation (90) can be expressed as:

$$\delta_N = \left[\left(\frac{1}{2 \Delta \sigma \Delta R} \right)^2 \frac{1}{n} \left(\frac{P_N^2}{P_{11}^2} + \frac{P_N^2}{P_{12}^2} + \frac{P_N^2}{P_{21}^2} + \frac{P_N^2}{P_{22}^2} \right) \right]^{\frac{1}{2}} \quad (91)$$

But the "on" and "off"-resonance powers are related by Equation (5):

$$P_{21} \exp \left\{ -2 \int_0^{R_1} N_{CO_2} \Delta \sigma dr \right\} + P_{11} \quad (92)$$

$$P_{22} \exp \left\{ -2 \int_0^R N_{CO_2} \Delta \sigma dr \right\} + P_{11} \quad (93)$$

Combining Equations (91), (92), and (93) gives:

$$\begin{aligned} \delta_N = & \left\{ \left(\frac{1}{2 \Delta \sigma \Delta R} \right)^2 \frac{1}{n} \left[\frac{1}{\left(\frac{S}{N} \right)_{H22}^2} (1 + \exp 4 \int_0^{R_2} N_{CO_2} \Delta \sigma dr) \right. \right. \\ & \left. \left. + \frac{1}{\left(\frac{S}{N} \right)_{H21}^2} (1 + \exp 4 \int_0^{R_1} N_{CO_2} \Delta \sigma dr) \right] \right\}^{\frac{1}{2}} \quad (94) \end{aligned}$$

From Appendices C and D, it can be determined that:

$$14.91 \sigma_2 = \sigma_1$$

Therefore, $\Delta \sigma = 13.91 \sigma_2$. Substituting this result into Equation (94), and using extinction coefficients for "off"-resonance CO_2 in Appendix H, and $\left(\frac{S}{N} \right)_{H_2}$ values in Table II, the standard deviation of the concentration in cm^{-3} and ppm can be calculated. These results are given in Table V. Clearly, this shows that even above 195km that the uncertainty of the measured concentration may preclude shuttle-borne lidar operation at the proposed frequencies, even though adequate signal-to-noise ratios are available.

These results do not generally compare to Korb (Ref. 17) From the spectrum in that abstract, the optical depth for the "on"-resonance frequency for a two kilometer horizontal path at sea level is given as:

$$K = 1 = \int_0^2 N_{CO_2} \sigma_1 \times 10^5 dr$$

For a sea level concentration of CO_2 of $8.405 \times 10^{15} \text{ cm}^{-3}$, the "on"-resonance cross section is solved as $\sigma_1 = 5.95 \times 10^{-22} \text{ cm}^2$. This does not agree well with the previously calculated value of $\sigma_1 = 2.029 \times 10^{-20} \text{ cm}^2$. If Korb's value of σ_1 is correct, then the error of measurement will be much less.

The fact that the error of the CO_2 concentration is so large is due to the large optical depth for the "on"-resonance frequency. This agrees with Remsberg and Gordley (Ref. 15), who predict that for an optical depth of greater than four, the on-line signal from the range cell will be small and difficult to measure.

Table V

Standard Deviation of N_{CO_2} at Various Altitudes

R_1 (km)	R_2 (km)	$\Delta\sigma$ (cm ²)	σ_N (cm ⁻³)	σ_N (ppm)
190	191	1.67×10^{-22}	8.596×10^{14}	99.98
191	192	2.87×10^{-22}	6.147×10^{14}	63.29
192	193	4.83×10^{-22}	5.802×10^{14}	53.08
193	194	7.94×10^{-22}	9.910×10^{14}	80.77
194	195	1.27×10^{-21}	4.395×10^{15}	80.77
195	196	1.99×10^{-21}	8.753×10^{16}	5.72×10^3
196	197	3.07×10^{-21}	3.391×10^{19}	1.99×10^6
197	198	4.63×10^{-21}	8.050×10^{23}	3.85×10^{10}
198	199	6.87×10^{-21}	1.123×10^{31}	5.36×10^{17}
199	200	1.00×10^{-20}	5.261×10^{44}	2.28×10^{31}

VI. Conclusions and Recommendations

Conclusions

On the basis of the above analysis the following conclusions are made:

1. A range-resolved differential absorption lidar is the only system capable of measuring concentrations of constituents of the troposphere.
2. Of the major interfering species in the atmosphere at 4.86μ (carbon monoxide, water, ozone, aerosols, and carbon dioxide), carbon dioxide provides the major contribution to the total extinction coefficient.
3. The minimum $\left(\frac{S}{N}\right)_2$ required is determined to be two. Direct detection could not produce this result due to the thermal noise of the detection system. Heterodyne detection, however, produces $\left(\frac{S}{N}\right)_2 \approx 8$ after increasing the bandwidth to 10^7 Hz.
4. Addition of hot CO_2 below 2km can be detected up to a maximum concentration of approximately 10^{15} cm^{-3} depending on altitude and temperature.
5. Error analysis of measured CO_2 concentrations indicates very large standard deviations particularly below five kilometers. This is due to the increased extinction of the laser beam due to

FD-164 308

DETECTION OF ATMOSPHERIC CARBON DIOXIDE FROM A
SHUTTLE-BORNE LIDAR(U) AIR FORCE INST OF TECH
WRIGHT-PATTERSON AFB OH SCHOOL OF ENGINEERING R H MANK
DEC 82 AFIT/GE/PH/82D-25 F/G 4/1

2/2

UNCLASSIFIED

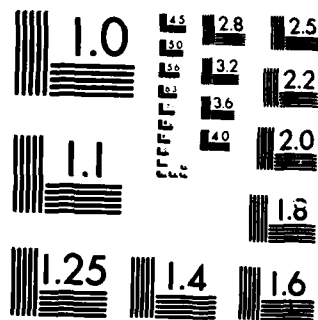
F/G 4/1

NL

End

2015년 12월 25일

L'Espresso



MICROCOPY RESOLUTION TEST CHART
NATIONAL BUREAU OF STANDARDS-1963-A

"on"-resonance absorption. This does not agree well with Korb's analysis whose "on"-resonance cross section is computed as approximately 34 times smaller than the cross section computed in this thesis.

Recommendations

Based on this thesis the following recommendations are made:

1. Update of the spectroscopic data of the 4.82μ absorption band of CO_2 should be made to determine the actual line intensities and widths so exact cross sections are readily available. This would determine whether the P(34) line is acceptable for "on"-resonance absorption, or whether another absorption line or band in combination with suitable laser would provide more meaningful results.
2. Even though this particular investigation did not provide suitable results to recommend a working system, it appears that a similar approach at another frequency in the 4.82μ spectral region could track CO_2 concentrations with relatively small error. It appears the system could be quite effective in locating sudden changes in CO_2 concentrations at a large industrial complex or laser facility.

Bibliography

1. Tuer, T.W. et al. Atmospheric Effects on Low Power Laser Beam Propagation. SAM-TR-80-51. Brooks AFB, Texas: USAF School of Aerospace Medicine, December 1980. (AD A095 383/6)
2. Bartman, Fred. High Altitude Balloon Flight Interferometer Data, High Resolution Spectra of CO₂ and Earth Atmosphere CO₂ Distribution Review. NASA-CR-109090. Ann Arbor, Michigan: University of Michigan, December 1969. (N70-20921)
3. Manquero, Carlos. An Indication from Satellite Measurements of Atmospheric CO₂ Variability. ECOM-5574. Ft. Monmouth, New Jersey: US Army Electronics Command, September 1975. (AD A017 057)
4. "Laser Monitoring of the Atmosphere" in Topics in Applied Physics, Volume 14, edited by E.D. Hinckley. Berlin, Heidelberg New York: Springer Verlag, 1976.
5. Smith, Irene. CO₂ and the Greenhouse Effect, An Unresolved Problem. London, England: IEA Coal Research, April 1978. (N80-11108/8)
6. Kellogg, W. W. and R Schwere. Climate Change and Society: Consequences of Increasing Atmospheric CO₂. DOE/EV/10281-T381-19 3982. Aspen, Colorado: Aspen Institute for Humanistic Studies, 1981.
7. Browell, Edward V. et al. Shuttle Atmospheric Lidar Research Program. NASA SP-433. Washington, DC: Langley Research Center, NASA, 1979.
8. Albanese, A.S. and M. Steinberg. Environmental Control Technology for Atmospheric CO₂. BNL-51116. September 1979.
9. Townes, Charles H. and Arthur L. Schawlow. Microwave Spectroscopy. New York: Dover Publications, Inc., 1975.
10. McClatchey, R.A. Atmospheric Absorption Line Parameters Compilation. AFCRL-TR-73-0096. L.G. Hanscom Field Bedford, Massachusetts: Air Force Cambridge Research Laboratories, January 1973.
11. Arcas, Phillipe and Eric Arie'. "Absorption Spectrum of Co₂ in the 4.86 μ m Region," Journal of Molecular Spectroscopy, 70; 134-142 (April 1978).

12. Kobayasi, Takao and Humio Inaba. "Spectroscopic Detection of SO₂ and CO₂ Molecules in Polluted Atmosphere by Laser-Raman Radar Technique," Applied Physics Letters, 17: 139-141 (August 1970).
13. McIlrath, T.J. "Fluorescence Lidar," Optical Engineering, 19: 494-502 (July/August 1980).
14. Kweder, Glenn C. Remote Sensing of Gases Using Lidar Resonance Scattering Techniques from the Space Shuttle. MS Thesis. Wright-Patterson AFB, Ohio: School Engineering, Air Force Institute of Technology, December 1981.
15. Remsberg, E.E. and L.L. Gordley. "Analysis of Differential Absorption Lidar from the Space Shuttle," Applied Optics, 17: 624-630 (February 1978).
16. Bernstein, L.S. et al. "Measured and Predicted Atmospheric Transmission in the 4.0-5.3 μ m Region, and Contribution of Continuum Absorption by CO₂ and N₂," Applied Optics, 18: 2454 (July 1979).
17. Korb, C.L. et al. "A Lidar Technique for Measurement of Atmospheric Carbon Dioxide," Proceedings of the Tenth International Laser Radar Conference. 105-106. Silver Springs, Maryland: Committee on Laser Atmospheric Studies, October 1980.
18. Measures, R.M. "Lidar Equation Analysis Allowing for Target Lifetime, Laser Pulse Duration, and Detector Integration Period," Applied Optics, 16: 1092-1103 (April 1977).
19. Thompson, Richard T. Differential Absorption and Scattering Sensitivity Predictions. NASA CR-2627. Norfolk, Virginia: Old Dominion University, August 1976.
20. Englisch, W. et al. Multidisciplinary Lidar System in Spacelab for Application to Atmospheric Physics and Remote Sensing. Paris, France: European Space Agency, December 1977.
21. Brockman, Philip et al. DIAL with Heterodyne Detection Including Speckle Noise: Aircraft/Shuttle Measurements of O₃, H₂O, and NH₃ with Pulsed Tunable CO₂ Lasers. NASA-TP-1725. August 1980. (80N29692).
22. Megie, G. and R.T. Menzies. "Complementarity of UV and IR Differential Absorption Lidar for Global Measurements of Atmospheric Species," Applied Optics, 19: 1173-1183 (April 1980).

23. Elterman, L. UV, Visible, and IR Attenuation for Altitudes to 50 km, 1968. AFCRL 68-0183. L.G. Hanscom Field Bedford, Massachusetts: Air Force Cambridge Research Laboratories, April 1968.
24. Byer, Robert L. and Max Garbuny. "Pollutant Detection by Absorption Using Mie Scattering and Topographic Targets as Retroreflectors," Applied Optics, 12: 1496-1505 (July 1973).
25. Shettle, Eric P. and Robert W. Fenn. "Models of the Atmospheric Aerosols and Their Optical Properties," Optical Propagation in the Atmosphere, AGARD Conference Proceedings No. 183. 2-1 - 2-16. Lyngby, Denmark: NATO Advisory Group for Aerospace Research and Development, October 1975.
26. Deirmendjian, D. "Scattering and Polarization Properties of Water Clouds and Hazes in the Visible and Infrared," Applied Optics, 3: 187-196.
27. Selby, J.E.A. and McClatchey, R.A. Atmospheric Transmittance from .25 to 28. μ m: Computer Code LOWTRAN 3. AFCRL-TR-75-0255. L.G. Hanscom Field Bedford, Massachusetts: Air Force Cambridge Research Laboratories, March 1982.
28. Burch, Darrell E. Continuum Absorption by H₂O. AFGL-TR-81-0300. L.G. Hanscom Field Bedford, Massachusetts: Air Force Cambridge Research Laboratories, March 1982.
29. Environmental Research Institute of Michigan. The Infrared Handbook, edited by William L. Wolfe and George J. Zissis. Washington, DC: Office of Naval Research, 1978.
30. Rothman, L.S. et al. "AFGL Trace Gas Compilation: 1980 Version," Applied Optics, 20: 1323-1328 (April 1981).
31. Rothman, Laurence S. and Louise D.G. Young. "IR Energy Levels and Intensities of CO₂-II," Journal of Quantum Spectroscopic Radiative Transfer, 25: 505-524 (1981).
32. Burch, Darrell E. et al. Investigation of the Absorption of Infrared Radiation by Atmosphere Gases. AFCRL-70-0373. L.G. Hanscom Field Bedford, Massachusetts: Air Force Cambridge Research Laboratories, June 1970.
33. Synder, David G. Tuned Diode Laser Measurements of Atmospheric Absorption Profiles in the 4.5 μ -5 μ Region. Research Triangle Park, North Carolina: US Army Research Office. (AD-A066 159)

34. Rothman, L.S. "AFGL Atmospheric Absorption Line Parameters Compilation: 1980 Version," Applied Optics, 20: 791-795 (March 1981).
35. Todd, T.R. et al. "Infrared Emission of $^{12}\text{C}^{16}\text{O}$, $^{13}\text{C}^{16}\text{O}$, and $^{12}\text{C}^{18}\text{O}$," Journal of Molecular Spectroscopy, 62: 201-227 (August 1976).
36. Flaud, J.M. and C. Camy-Peyret. Water Vapour Line Parameters from Microwave to Medium Infrared: (And Intensities Between 0 and 4350ma). New York: Pergamon Press, 1981.
37. Flaud, J.M. et al. "Line Positions and Intensities of the $2\nu_3$, $\nu_1 + \nu_3$, and $2\nu_1$ Bands of Ozone," Journal of Molecular Spectroscopy, 80: 185-199 (March 1980).
38. Nickerson, Gary R. Nonequilibrium Radiation Model for Exhaust Plumes. Air Force Rocket Propulsion Laboratory, March 1975. (Ad-A007795)
39. United States Committee on Extension to the Standard Atmosphere. U.S. Standard Atmosphere, 1976. Washington, D.C.: NOAA, NASA, USAF, October 1976.
40. Pivovonsky, Mark and Max R. Nagel. Tables of Blackbody Radiation Functions. New York: MacMillan Co., 1961.
41. Hengehold, R., Professor of Physics. Lecture materials distributed in PH6.42, Optical Diagnostics Laboratory. School of Engineering, Air Force Institute of Technology, Wright-Patterson AFB, Ohio, 1982.
42. Bell, E.E. et al. "Spectral Radiance of Sky and Terrain at Wavelengths Between 1 and 20 Microns," Journal of the Optical Society of America, 50: 1313-1320 (December 1971).
43. Byer, Robert L. and Helge Kildal. "Comparison of Laser Methods for the Remote Detection of Atmosphere Pollutants," Proceedings of the IEEE, 59: 1663-1664 (December 1971).
44. Kruse, P.W. "Optical and Infrared Detectors" in Topics in Applied Physics, Volume 19, edited by R.J. Keyes. Berlin Heidelberg New York: Springer-Verlag, 1980.

45. Cruickshank, J.M. "Transversely Excited Atmospheric CO₂ Laser Radar With Heterodyne Detection," Applied Optics, 18: 290-293 (February 1979).
46. Lundquist, Stefan et al. "Air Pollution Monitoring With a Q-Switched CO₂-Laser Lidar Using Heterodyne Detection," Applied Optics, 20: 2534-2538 (July 1981).
47. Kingston, R.H. "Detection of Optical and Infrared Radiation" in Springer Series in Optical Sciences, Volume 10, edited by David L. MacAdam. Berlin Heidelberg New York: Springer-Verlag, 1978.
48. Elbaum, Marek and Malvin Teich. "Heterodyne Detection of Random Gaussian Signals in the Optical and Infrared: Optimization of Pulse Duration," Optics Communications, 27: 257-261 (November 1978).
49. Pedrotti, L.S., Professor of Physics. Lecture materials distributed in PH7.43, Laser Physics I. School of Engineering, Air Force Institute of Technology, Wright-Patterson AFB, Ohio, 1982.
50. Herzberg, G. Infrared and Raman Spectra. Princeton, New Jersey: D. van Nostrand Co., 1947.
51. Case, C.T. and Pedrotti, L.S., Professors of Physics. Lecture materials distributed in PH6.61, Atomic and Molecular Physics. School of Engineering, Air Force Institute of Technology, Wright-Patterson AFB, Ohio, 1981.
52. Douglas-Hamilton, D.H. et al. Carbon Dioxide Electric Discharge Laser Kinetics Handbook. AFWL-TR-74-216. Kirtland AFB, New Mexico: USAF Weapons Laboratory, April 1975. (AD-A008 650)
53. McClatchey, R.A. and J.E.A. Selby. Atmospheric Attenuation of HF and DF Laser Radiation. AFCRL-72-0312. L.G. Hanscom Field Bedford, Massachusetts: Air Force Cambridge research Laboratories, May 1972.
54. Mills, F.S. Absorption of Deuterium Fluoride Laser Radiation by the Atmosphere. RADC-76-105. Griffith AFB, New York: Rome Air Development Center, April 1976. (AD A025 402)

55. Deaton, Terrance F., David A Depatie, and Thomas W. Walker. "Absorption Coefficient Measurement of Nitrous Oxide and Methane at DF Laser Wavelengths," Applied Physics Letters, 26: 300-303 (March 1975).
56. McClatchey, R.A. Atmospheric Attenuation of CO Laser Radiation. AFCRL 71-0370. L.G. Hanscom Field Bedford, Massachusetts: Air Force Cambridge Research Laboratories, July 1971.
57. Ford, D.L. Laser Absorption in the 5 Micron Band. RADC-TR-72-140. Griffith AFB, New York: Rome Air Development Center, April 1972. (AD 745 585)
58. Ford, D.L., F.S. Mills, and P.K. Long. Laser Absorption in the 5 Micron Band. RADC-TR-72-195. Griffith AFB, New York: Rome Air Development Center, July 1972. (AD 748 437)
59. Long, R.K., F.S. Mills, and G.L. Trusty. Experimental Absorption Coefficients for Eleven CO Laser Lines. RADC-TR-73-126. Griffith AFB, New York: Rome Air Development Center, 1973. (AD 760 140)

APPENDICES

Appendix A

Raleigh Scattering Coefficients

<u>h (km)</u>	<u>$\xi_{2R} (\text{km}^{-1})$</u>	<u>h (km)</u>	<u>$\xi_{2R} (\text{km}^{-1})$</u>
0	1.909×10^{-6}	20	1.386×10^{-7}
1	1.732×10^{-6}	21	1.180×10^{-7}
2	1.568×10^{-6}	22	1.005×10^{-7}
3	1.417×10^{-6}	23	8.573×10^{-8}
4	1.277×10^{-6}	24	7.314×10^{-8}
5	1.147×10^{-6}	25	6.246×10^{-8}
6	1.029×10^{-6}	26	5.338×10^{-8}
7	9.195×10^{-7}	27	4.565×10^{-8}
8	8.191×10^{-7}	28	3.907×10^{-8}
9	7.278×10^{-7}	29	3.347×10^{-8}
10	6.443×10^{-7}	30	2.869×10^{-8}
11	5.684×10^{-7}	31	2.460×10^{-8}
12	4.861×10^{-7}	32	2.112×10^{-8}
13	4.154×10^{-7}	33	1.803×10^{-8}
14	3.551×10^{-7}	34	1.541×10^{-8}
15	3.034×10^{-7}	35	1.319×10^{-8}
16	2.594×10^{-7}	36	1.131×10^{-8}
17	2.217×10^{-7}	37	9.712×10^{-9}
18	1.895×10^{-7}	38	8.363×10^{-9}
19	1.602×10^{-7}	39	7.209×10^{-9}

$h \text{ (km)}$	$\xi_{2R} \text{ (km}^{-1}\text{)}$
40	6.226×10^{-9}
41	5.386×10^{-9}
42	4.667×10^{-9}
43	4.050×10^{-9}
44	3.520×10^{-9}
45	3.064×10^{-9}
46	2.621×10^{-9}
47	2.332×10^{-9}
48	2.052×10^{-9}
49	1.812×10^{-9}
50	1.600×10^{-9}

Appendix B

Mie Scattering and Extinction Coefficients (4.86μ)

(Urban/Rural)

<u>h(km)</u>	<u>Extinction Coefficient</u> (km ⁻¹)	<u>Scattered Coefficient</u> (km ⁻¹)
0	.023/.016	.010/.013
1	1.48 x 10 ⁻² /1.03 x 10 ⁻³	6.45 x 10 ⁻³ /8.39 x 10 ⁻³
2	8.90 x 10 ⁻³ /6.19 x 10 ⁻³	3.87 x 10 ⁻³ /5.03 x 10 ⁻³
3	7.23 x 10 ⁻⁴	4.65 x 10 ⁻⁴
4	3.61 x 10 ⁻⁴	2.32 x 10 ⁻⁴
5	2.17 x 10 ⁻⁴	1.39 x 10 ⁻⁴
6	1.45 x 10 ⁻⁴	9.29 x 10 ⁻⁵
7	9.94 x 10 ⁻⁵	6.39 x 10 ⁻⁵
8	5.42 x 10 ⁻⁵	3.48 x 10 ⁻⁵
9	3.07 x 10 ⁻⁵	1.97 x 10 ⁻⁵
10	4.74 x 10 ⁻⁵	3.07 x 10 ⁻⁵
11	3.61 x 10 ⁻⁵	
12	2.48 x 10 ⁻⁵	
13	2.03 x 10 ⁻⁵	
14	1.94 x 10 ⁻⁵	
15	1.90 x 10 ⁻⁵	
16	1.94 x 10 ⁻⁵	
17	1.99 x 10 ⁻⁵	
18	2.12 x 10 ⁻⁵	
19	2.48 x 10 ⁻⁵	
20	2.71 x 10 ⁻⁵	

<u>h(km)</u>	<u>Extinction Coefficient</u> (km^{-1})
21	2.48×10^{-5}
22	1.81×10^{-5}
23	1.35×10^{-5}
24	8.58×10^{-6}
25	5.42×10^{-6}
26	3.61×10^{-6}
27	3.16×10^{-6}
28	2.26×10^{-6}
29	1.81×10^{-6}
30	1.35×10^{-6}

Appendix C

CO₂ Absorption Cross Section ("On"-Resonance)

<u>Rot. ID</u>	<u>ν_0 (cm⁻¹)</u>	<u>S_m (cm⁻¹ mol⁻¹ cm⁻²)</u>	<u>σ_{1CO_2} (cm²)</u>
P(34)	2050.568	5.140 x 10 ⁻²¹	2.015 x 10 ⁻²⁰
P(36)	2049.043	4.916 x 10 ⁻²¹	4.532 x 10 ⁻²³
P(38)	2047.512	4.662 x 10 ⁻²¹	1.092 x 10 ⁻²³
P(40)	2045.988	4.382 x 10 ⁻²¹	4.597 x 10 ⁻²⁴
P(32)	2052.106	5.332 x 10 ⁻²¹	5.199 x 10 ⁻²³
P(30)	2053.631	5.491 x 10 ⁻²¹	1.328 x 10 ⁻²³
P(28)	2055.175	5.613 x 10 ⁻²¹	5.963 x 10 ⁻²⁴
P(26)	2056.705	5.699 x 10 ⁻²¹	3.402 x 10 ⁻²⁴
P(24)	2058.247	5.747 x 10 ⁻²¹	2.187 x 10 ⁻²⁴
P(22)	2059.781	5.757 x 10 ⁻²¹	1.520 x 10 ⁻²⁴
P(20)	2061.332	5.728 x 10 ⁻²¹	1.107 x 10 ⁻²⁴
P(18)	2062.868	5.662 x 10 ⁻²¹	8.377 x 10 ⁻²⁵
P(42)	2044.464	4.078 x 10 ⁻²¹	2.416 x 10 ⁻²⁴
P(44)	2042.946	3.753 x 10 ⁻²¹	1.429 x 10 ⁻²⁴
P(46)	2041.433	3.500 x 10 ⁻²¹	9.287 x 10 ⁻²⁵
Total σ_{1CO_2}			<u>$= 2.029 \times 10^{-20} \text{ cm}^2$</u>

Appendix D

CO₂ Absorption Cross Section ("Off"-Resonance)

<u>Rot. ID</u>	<u>ν_o (cm⁻¹)</u>	<u>S_m (cm⁻¹ mol⁻¹ cm⁻²)</u>	<u>σ_{2CO_2} (cm²)</u>
P(34)	2050.568	5.140 x 10 ⁻²¹	2.747 x 10 ⁻²⁴
P(26)	2056.705	5.699 x 10 ⁻²¹	1.191 x 10 ⁻²¹
P(24)	2058.247	5.747 x 10 ⁻²¹	8.5328 x 10 ⁻²³
P(28)	2055.175	5.613 x 10 ⁻²¹	3.653 x 10 ⁻²³
P(22)	2059.781	5.757 x 10 ⁻²¹	1.686 x 10 ⁻²³
P(30)	2053.631	5.491 x 10 ⁻²¹	1.062 x 10 ⁻²³
P(20)	2061.332	5.728 x 10 ⁻²¹	6.875 x 10 ⁻²⁴
P(32)	2052.106	5.322 x 10 ⁻²¹	4.911 x 10 ⁻²⁴
P(18)	2062.868	5.662 x 10 ⁻²¹	3.693 x 10 ⁻²⁴
P(36)	2049.043	4.916 x 10 ⁻²¹	1.719 x 10 ⁻²⁴
P(382)	2047.512	4.662 x 10 ⁻²¹	1.148 x 10 ⁻²⁴
Total σ_{2CO_2} =			1.361 x 10 ⁻²¹

Appendix E

CO Absorption Cross Section ("Off"-Resonance)

<u>Rot. ID</u>	<u>ν_0 (cm⁻¹)</u>	<u>S_m (cm² mol⁻¹ cm⁻¹)</u>	<u>σ_{2CO} (cm²)</u>
P(20)	2059.9151	3.703×10^{-20}	8.457×10^{-23}
P(21)	2055.4008	2.620×10^{-20}	1.897×10^{-22}
P(22)	2050.8545	1.819×10^{-20}	9.126×10^{-24}
P(23)	2046.2765	1.234×10^{-20}	2.047×10^{-24}
P(24)	2041.668	8.229×10^{-21}	6.66×10^{-25}
P(19)	2064.3973	5.118×10^{-20}	1.797×10^{-23}
P(18)	2068.8474	6.903×10^{-20}	9.431×10^{-24}
P(17)	2073.2650	9.189×10^{-20}	6.65×10^{-24}
P(16)	2077.6502	1.189×10^{-19}	5.34×10^{-24}
P(15)	2082.0027	1.504×10^{-19}	4.60×10^{-24}
P(14)	2086.3224	1.861×10^{-19}	4.14×10^{-24}
P(13)	2090.6091	2.254×10^{-19}	3.82×10^{-24}
P(12)	2094.8628	2.661×10^{-19}	3.54×10^{-24}
P(11)	2099.0832	3.063×10^{-19}	3.31×10^{-24}
P(10)	2103.2702	3.443×10^{-19}	3.07×10^{-24}
P(9)	2107.4237	3.744×10^{-19}	2.82×10^{-24}
P(8)	2111.5435	3.964×10^{-19}	2.54×10^{-24}
P(7)	2115.6294	4.064×10^{-19}	2.267×10^{-24}
P(6)	2119.6814	4.014×10^{-19}	1.95×10^{-24}
P(5)	2123.6993	3.799×10^{-19}	1.63×10^{-24}

$$\text{Total } \sigma_{2CO} = 3.585 \times 10^{-22}$$

Appendix F

H₂O Absorption Cross Section ("Off"-Resonance)

<u>ν_o (cm⁻¹)</u>	<u>S_m (cm⁻¹ mol⁻¹ cm²)</u>	<u>σ_{2H_2O} (cm²)</u>
2057.408	.235 x 10 ⁻²⁴	1.612 x 10 ⁻²⁶
2057.410	.414 x 10 ⁻²⁵	2.811 x 10 ⁻²⁷
2056.516	.279 x 10 ⁻²⁵	1.097 x 10 ⁻²⁷
2058.239	.223 x 10 ⁻²⁴	1.539 x 10 ⁻²⁷
2055.910	.138 x 10 ⁻²⁵	1.133 x 10 ⁻²⁸
2058.495	.122 x 10 ⁻²⁴	5.743 x 10 ⁻²⁸
2058.653	.241 x 10 ⁻²⁵	9.251 x 10 ⁻²⁹
2054.555	.419 x 10 ⁻²⁵	7.001 x 10 ⁻²⁹
2054.431	.127 x 10 ⁻²³	1.924 x 10 ⁻²⁷
2058.877	.409 x 10 ⁻²⁵	1.201 x 10 ⁻²⁸
2059.092	.366 x 10 ⁻²⁴	8.717 x 10 ⁻²⁸
2053.862	.412 x 10 ⁻²³	4.197 x 10 ⁻²⁷
2053.165	.124 x 10 ⁻²⁵	8.48 x 10 ⁻³⁰
2053.047	.722 x 10 ⁻²⁵	4.650 x 10 ⁻²⁹
2059.107	.497 x 10 ⁻²⁵	1.167 x 10 ⁻²⁸
2059.215	.673 x 10 ⁻²⁵	1.428 x 10 ⁻²⁸
2059.759	.132 x 10 ⁻²⁴	1.797 x 10 ⁻²⁸
2060.484	.352 x 10 ⁻²¹	2.995 x 10 ⁻²⁵
2060.646	.108 x 10 ⁻²⁴	8.385 x 10 ⁻²⁹
2060.715	.232 x 10 ⁻²⁴	2.415 x 10 ⁻²⁸
2052.410	.127 x 10 ⁻²⁵	6.077 x 10 ⁻³⁰

2051.993	.808 x 10 ⁻²⁵	3.252 x 10 ⁻²⁹
2062.149	.858 x 10 ⁻²⁵	3.327 x 10 ⁻²⁹
2061.875	.368 x 10 ⁻²⁴	1.593 x 10 ⁻²⁸
2062.549	.779 x 10 ⁻²⁴	2.599 x 10 ⁻²⁸
2062.557	.26 x 10 ⁻²⁴	8.651 x 10 ⁻²⁹
2063.078	.567 x 10 ⁻²⁴	1.576 x 10 ⁻²⁸
2063.089	.342 x 10 ⁻²⁵	9.470 x 10 ⁻³⁰
2063.113	.279 x 10 ⁻²⁴	7.665 x 10 ⁻²⁹
2051.557	.29 x 10 ⁻²³	9.883 x 10 ⁻²⁸
2051.388	.131 x 10 ⁻²³	4.201 x 10 ⁻²⁸
2051.046	.347 x 10 ⁻²⁴	9.890 x 10 ⁻²⁹
2050.986	.294 x 10 ⁻²⁴	8.214 x 10 ⁻²⁹
2050.649	.106 x 10 ⁻²³	2.657 x 10 ⁻²⁹
2064.853	.499 x 10 ⁻²¹	8.923 x 10 ⁻²⁶
2064.854	.150 x 10 ⁻²⁰	2.492 x 10 ⁻²⁵
2065.021	.199 x 10 ⁻²¹	3.170 x 10 ⁻²⁶
2065.644	.156 x 10 ⁻²⁴	2.139 x 10 ⁻²⁹
2065.846	.595 x 10 ⁻²¹	7.787 x 10 ⁻²⁶
2049.730	.723 x 10 ⁻²⁴	1.384 x 10 ⁻²⁸
2048.649	.270 x 10 ⁻²³	3.921 x 10 ⁻²⁸
2047.725	.201 x 10 ⁻²⁴	2.368 x 10 ⁻²⁹
2046.796	.369 x 10 ⁻²³	3.593 x 10 ⁻²⁸
2046.516	.126 x 10 ⁻²¹	1.162 x 10 ⁻²⁶
2046.486	.114 x 10 ⁻²⁴	1.046 x 10 ⁻²⁹
2066.614	.349 x 10 ⁻²⁴	3.865 x 10 ⁻²⁹
2067.778	.250 x 10 ⁻²³	2.202 x 10 ⁻²⁸

2068.896	.159 x 10 ⁻²⁴	1.149 x 10 ⁻²⁹
2070.683	.113 x 10 ⁻²⁴	5.356 x 10 ⁻³⁰
2043.951	.401 x 10 ⁻²¹	2.390 x 10 ⁻²⁶
2043.943	.652 x 10 ⁻²⁴	3.881 x 10 ⁻²⁹
2043.698	.142 x 10 ⁻²⁴	8.145 x 10 ⁻³⁰
2043.165	.148 x 10 ⁻²⁴	8.489 x 10 ⁻³⁰
2041.513	.396 x 10 ⁻²²	1.677 x 10 ⁻²⁷
2041.497	.520 x 10 ⁻²¹	2.197 x 10 ⁻²⁶
2041.289	.156 x 10 ⁻²⁰	6.418 x 10 ⁻²⁶
2071.950	.847 x 10 ⁻²⁴	3.873 x 10 ⁻²⁹
2072.003	.403 x 10 ⁻²⁴	1.830 x 10 ⁻²⁹
2072.488	.124 x 10 ⁻²⁴	5.28 x 10 ⁻³⁰
2072.541	.167 x 10 ⁻²²	7.065 x 10 ⁻²⁸
2073.379	.186 x 10 ⁻²³	7.083 x 10 ⁻²⁹
2073.990	.526 x 10 ⁻²³	1.861 x 10 ⁻²⁸
2074.253	.181 x 10 ⁻²¹	6.379 x 10 ⁻²⁷
2074.689	.145 x 10 ⁻²⁴	4.733 x 10 ⁻³⁰
2040.306	.171 x 10 ⁻²⁴	6.232 x 10 ⁻³⁰
2040.016	.859 x 10 ⁻²⁴	3.025 x 10 ⁻²⁹
2039.946	.347 x 10 ⁻²³	1.212 x 10 ⁻²⁸
2039.292	.145 x 10 ⁻²⁴	4.697 x 10 ⁻³⁰
2038.094	.989 x 10 ⁻²⁴	2.811 x 10 ⁻²⁹
2037.507	.113 x 10 ⁻²¹	3.022 x 10 ⁻²⁷
2036.620	.252 x 10 ⁻²⁴	6.166 x 10 ⁻³⁰
2057.629	.106 x 10 ⁻²⁴	3.119 x 10 ⁻³⁰
2076.030	.46 x 10 ⁻²⁴	1.297 x 10 ⁻²⁹

2076.698	.315 x 10 ⁻²⁴	8.289 x 10 ⁻³⁰
2076.973	.483 x 10 ⁻²³	1.236 x 10 ⁻²⁸
2077.041	.114 x 10 ⁻²⁴	2.898 x 10 ⁻³⁰
2053.530	.194 x 10 ⁻²⁴	4.227 x 10 ⁻³⁰
2035.309	.582 x 10 ⁻²⁴	1.257 x 10 ⁻²⁹
2035.149	.785 x 10 ⁻²⁴	1.671 x 10 ⁻²⁹
2034.360	.898 x 10 ⁻²⁴	1.781 x 10 ⁻²⁹
2034.191	.134 x 10 ⁻²⁴	2.618 x 10 ⁻³⁰
2034.141	.267 x 10 ⁻²²	5.194 x 10 ⁻²⁹
2034.054	.445 x 10 ⁻²²	8.591 x 10 ⁻²⁸
2034.034	.314 x 10 ⁻²³	6.051 x 10 ⁻²⁹
2032.290	.123 x 10 ⁻²³	2.048 x 10 ⁻²⁹
2078.570	.103 x 10 ⁻²¹	2.260 x 10 ⁻²⁷
2079.932	.376 x 10 ⁻²³	7.298 x 10 ⁻²⁹
2081.874	.457 x 10 ⁻²²	7.538 x 10 ⁻²⁸
2085.494	.141 x 10 ⁻²³	1.722 x 10 ⁻²⁹
2087.408	.205 x 10 ⁻²¹	2.262 x 10 ⁻²⁷
2027.025	.67 x 10 ⁻²²	7.017 x 10 ⁻²⁸
2026.603	.179 x 10 ⁻²¹	1.970 x 10 ⁻²⁷
2023.030	.421 x 10 ⁻²¹	3.711 x 10 ⁻²⁷
2019.071	.577 x 10 ⁻²¹	4.080 x 10 ⁻²⁷
2018.338	.117 x 10 ⁻²⁰	7.963 x 10 ⁻²⁷
2016.836	.367 x 10 ⁻²⁰	2.315 x 10 ⁻²⁶
2016.799	.122 x 10 ⁻²⁰	7.680 x 10 ⁻²⁷
2009.333	.197 x 10 ⁻²¹	8.823 x 10 ⁻²⁸
2007.701	.407 x 10 ⁻²¹	1.702 x 10 ⁻²⁷

2089.742	$.724 \times 10^{-22}$	6.889×10^{-28}
2090.023	$.676 \times 10^{-22}$	6.323×10^{-28}
2090.102	$.623 \times 10^{-21}$	5.800×10^{-27}
2090.107	$.208 \times 10^{-21}$	1.936×10^{-27}
2097.368	$.478 \times 10^{-22}$	2.991×10^{-28}
2100.433	$.543 \times 10^{-22}$	2.935×10^{-28}
2106.347	$.210 \times 10^{-22}$	8.793×10^{-29}
2107.547	$.210 \times 10^{-22}$	8.380×10^{-29}
2114.427	$.614 \times 10^{-22}$	1.898×10^{-28}
2115.018	$.234 \times 10^{-21}$	7.087×10^{-28}

$$\text{Total } \sigma_{2\text{H}_2\text{O}} = 9.85 \times 10^{-25}$$

Appendix G

O₃ Absorption Cross Section ("Off"-Resonance)

<u>ν_o (cm⁻¹)</u>	<u>S_i (cm⁻¹ mol⁻¹ cm²)</u>	<u>σ_{20_3} (cm²)</u>
2056.986	2.56 x 10 ⁻²³	6.618 x 10 ⁻²³
2057.054	5.77 x 10 ⁻²³	1.554 x 10 ⁻²²
2056.982	9.35 x 10 ⁻²³	2.361 x 10 ⁻²²
2056.081	3.13 x 10 ⁻²³	7.410 x 10 ⁻²³
2056.927	5.81 x 10 ⁻²³	9.45 x 10 ⁻²³
2057.135	5.89 x 10 ⁻²³	8.445 x 10 ⁻²³
2056.847	8.94 x 10 ⁻²⁴	7.208 x 10 ⁻²⁴
2057.163	1.65 x 10 ⁻²²	2.298 x 10 ⁻²²
2056.831	2.08 x 10 ⁻²³	1.476 x 10 ⁻²³
2057.174	1.09 x 10 ⁻²³	1.103 x 10 ⁻²³
2056.778	4.44 x 10 ⁻²³	2.140 x 10 ⁻²³
2057.235	5.37 x 10 ⁻²³	3.321 x 10 ⁻²³
2056.773	6.74 x 10 ⁻²⁴	3.142 x 10 ⁻²⁴
2057.284	1.49 x 10 ⁻²²	6.546 x 10 ⁻²³
2056.767	4.23 x 10 ⁻²³	1.895 x 10 ⁻²³
2057.299	1.40 x 10 ⁻²³	5.588 x 10 ⁻²⁴
2058.803	1.40 x 10 ⁻²²	1.547 x 10 ⁻²⁴
2055.160	3.78 x 10 ⁻²³	3.839 x 10 ⁻²⁵
2058.835	1.74 x 10 ⁻²³	1.85 x 10 ⁻²⁵
2055.135	3.43 x 10 ⁻²³	3.362 x 10 ⁻²⁵
2058.914	8.20 x 10 ⁻²³	8.029 x 10 ⁻²⁵

2055.000	1.03×10^{-23}	8.795×10^{-26}
2058.971	2.90×10^{-23}	2.676×10^{-25}
2054.929	2.76×10^{-23}	2.200×10^{-25}
2059.022	1.54×10^{-23}	1.349×10^{-25}
2054.782	1.27×10^{-23}	8.840×10^{-26}
2059.086	1.70×10^{-22}	1.399×10^{-24}
2054.754	1.01×10^{-22}	6.858×10^{-25}
2059.124	1.00×10^{-22}	7.933×10^{-25}
2054.722	1.56×10^{-23}	1.030×10^{-25}
2059.180	8.11×10^{-24}	2.104×10^{-26}
2054.621	3.84×10^{-23}	2.327×10^{-25}
2059.188	1.97×10^{-22}	1.472×10^{-24}
2054.558	6.76×10^{-24}	3.890×10^{-26}
2059.208	5.90×10^{-24}	4.327×10^{-26}
2054.498	1.26×10^{-23}	6.910×10^{-26}
2059.251	1.51×10^{-23}	1.065×10^{-25}
2054.466	9.00×10^{-24}	4.813×10^{-26}
2059.328	2.07×10^{-22}	1.364×10^{-24}
2054.436	1.77×10^{-23}	9.248×10^{-26}
2059.351	5.92×10^{-23}	3.825×10^{-25}
2054.430	9.97×10^{-23}	5.185×10^{-25}
2059.359	1.36×10^{-23}	8.728×10^{-26}
2054.395	8.40×10^{-23}	4.253×10^{-25}
2059.376	2.14×10^{-22}	1.354×10^{-24}
2054.360	8.53×10^{-24}	4.206×10^{-26}
2059.447	1.87×10^{-23}	1.115×10^{-25}

2054.295	6.51×10^{-23}	3.059×10^{-25}
2059.507	5.09×10^{-24}	2.889×10^{-26}
2054.292	1.19×10^{-22}	5.580×10^{-25}
2089.519	5.28×10^{-23}	2.968×10^{-25}
2054.290	4.12×10^{-23}	1.929×10^{-25}
2059.523	8.26×10^{-24}	4.268×10^{-26}
2054.216	3.92×10^{-23}	1.740×10^{-25}
2059.545	6.04×10^{-24}	3.326×10^{-26}
2054.171	2.35×10^{-23}	1.010×10^{-25}
2059.597	9.47×10^{-23}	5.00×10^{-25}
2054.141	3.93×10^{-23}	1.655×10^{-25}
2059.691	3.95×10^{-23}	1.943×10^{-25}
2054.073	3.92×10^{-23}	1.575×10^{-25}
2059.704	5.73×10^{-23}	2.792×10^{-25}
2054.030	7.49×10^{-23}	2.924×10^{-25}
2059.707	6.80×10^{-23}	3.306×10^{-25}
2054.028	6.64×10^{-23}	2.589×10^{-25}
2059.715	3.69×10^{-23}	1.783×10^{-25}
2053.987	5.37×10^{-24}	2.038×10^{-26}
2059.736	5.23×10^{-24}	2.489×10^{-26}
2053.944	1.16×10^{-23}	4.480×10^{-26}
2053.944	1.42×10^{-23}	5.240×10^{-26}
2059.770	2.22×10^{-23}	1.030×10^{-25}
2059.879	1.29×10^{-22}	5.539×10^{-25}
2053.907	4.11×10^{-23}	1.481×10^{-25}
2059.942	4.10×10^{-23}	1.685×10^{-25}

2053.859	2.14×10^{-23}	7.477×10^{-26}
2059.948	1.37×10^{-23}	5.608×10^{-26}
2053.809	1.87×10^{-23}	6.332×10^{-26}
2059.964	6.03×10^{-23}	2.442×10^{-25}
2053.800	1.47×10^{-23}	4.950×10^{-26}
2060.037	2.97×10^{-23}	1.145×10^{-25}
2053.783	1.07×10^{-23}	3.565×10^{-26}
2060.115	2.13×10^{-22}	7.803×10^{-25}
2053.553	1.01×10^{-22}	2.934×10^{-25}
2053.463	1.08×10^{-22}	2.898×10^{-25}
2060.258	1.64×10^{-22}	5.488×10^{-25}
2060.348	1.78×10^{-22}	5.639×10^{-25}
2060.616	1.98×10^{-22}	5.372×10^{-25}
2056.697	6.86×10^{-23}	2.018×10^{-23}
2057.309	2.33×10^{-23}	8.742×10^{-24}
2056.609	3.98×10^{-23}	7.560×10^{-24}
2057.340	1.64×10^{-23}	5.129×10^{-24}
2056.546	1.21×10^{-23}	1.761×10^{-24}
2057.354	1.19×10^{-22}	3.444×10^{-23}
2056.534	3.13×10^{-23}	4.346×10^{-24}
2057.387	9.34×10^{-23}	2.273×10^{-23}
2056.519	9.67×10^{-24}	1.167×10^{-24}
2056.456	1.47×10^{-22}	1.577×10^{-23}
2057.543	7.54×10^{-24}	9.663×10^{-25}
2057.543	1.20×10^{-23}	1.538×10^{-24}
2056.445	1.51×10^{-22}	1.522×10^{-23}

2057.605	1.57×10^{-23}	1.610×10^{-24}
2056.403	9.59×10^{-24}	8.621×10^{-25}
2057.697	1.11×10^{-23}	8.581×10^{-25}
2056.352	1.45×10^{-23}	1.115×10^{-24}
2057.711	1.43×10^{-22}	1.034×10^{-23}
2056.217	1.41×10^{-22}	7.536×10^{-24}
2057.733	8.94×10^{-24}	6.180×10^{-25}
2056.196	1.58×10^{-23}	8.024×10^{-25}
2057.907	1.67×10^{-23}	7.373×10^{-25}
2056.125	1.22×10^{-22}	5.260×10^{-24}
2057.970	1.59×10^{-23}	6.194×10^{-25}
2055.971	9.19×10^{-24}	2.892×10^{-25}
2057.991	1.68×10^{-22}	6.265×10^{-24}
2055.924	1.44×10^{-23}	4.154×10^{-25}
2058.058	3.45×10^{-23}	1.126×10^{-24}
2055.878	2.03×10^{-23}	5.396×10^{-25}
2058.071	4.60×10^{-23}	1.464×10^{-24}
2055.867	1.00×10^{-22}	2.608×10^{-24}
2058.101	1.65×10^{-22}	4.964×10^{-24}
2055.772	9.68×10^{-24}	2.157×10^{-24}
2058.122	3.53×10^{-23}	1.022×10^{-24}
2055.751	1.42×10^{-22}	3.061×10^{-24}
2058.152	7.48×10^{-24}	2.052×10^{-25}
2055.733	4.60×10^{-23}	9.642×10^{-25}
2058.154	8.08×10^{-23}	2.209×10^{-24}
2055.718	1.31×10^{-22}	2.683×10^{-24}

2058.243	4.93×10^{-23}	1.1587×10^{-24}
2055.683	8.50×10^{-23}	1.651×10^{-24}
2058.312	2.16×10^{-23}	4.548×10^{-25}
2055.632	2.72×10^{-23}	4.905×10^{-25}
2058.335	6.88×10^{-24}	1.398×10^{-25}
2055.572	5.88×10^{-24}	9.748×10^{-26}
2058.369	9.30×10^{-23}	1.796×10^{-24}
2055.489	4.88×10^{-23}	7.240×10^{-25}
2058.380	5.19×10^{-23}	9.862×10^{-25}
2055.484	7.70×10^{-23}	1.135×10^{-24}
2058.390	2.19×10^{-23}	4.101×10^{-25}
2055.432	2.35×10^{-23}	3.242×10^{-23}
2058.517	3.59×10^{-23}	5.629×10^{-25}
2055.384	6.03×10^{-24}	7.839×10^{-26}
2058.521	2.77×10^{-23}	9.320×10^{-24}
2055.355	3.87×10^{-23}	4.858×10^{-25}
2058.566	1.23×10^{-25}	1.808×10^{-25}
2055.333	1.98×10^{-23}	2.42×10^{-25}
2058.576	5.24×10^{-23}	7.61×10^{-25}
2055.321	1.15×10^{-23}	1.386×10^{-25}
2058.596	1.94×10^{-22}	2.744×10^{-24}
2055.319	6.36×10^{-23}	7.650×10^{-25}
2058.603	6.78×10^{-23}	9.507×10^{-25}
2055.276	3.60×10^{-23}	4.120×10^{-25}
2058.627	1.86×10^{-22}	2.531×10^{-24}
2055.246	1.02×10^{-22}	1.128×10^{-24}

2058.724	6.24×10^{-23}	7.550×10^{-25}
2055.225	6.80×10^{-23}	7.348×10^{-25}
2058.728	2.65×10^{-23}	3.191×10^{-25}
2055.220	1.78×10^{-23}	1.913×10^{-25}
2058.744	1.86×10^{-23}	2.199×10^{-25}
2055.162	1.17×10^{-22}	1.180×10^{-24}
2060.677	1.07×10^{-22}	2.807×10^{-25}
2060.798	2.41×10^{-22}	5.923×10^{-25}
2060.869	1.05×10^{-22}	2.486×10^{-25}
2060.991	2.30×10^{-22}	5.116×10^{-25}
2061.026	1.11×10^{-22}	2.426×10^{-25}
2061.324	1.10×10^{-22}	2.083×10^{-25}
2061.355	1.41×10^{-22}	2.631×10^{-25}
2061.488	20.58×10^{-22}	4.532×10^{-25}
2061.683	1.92×10^{-22}	3.097×10^{-25}
2061.813	1.88×10^{-22}	2.870×10^{-25}
2061.989	2.33×10^{-22}	3.301×10^{-25}
2062.109	2.71×10^{-22}	3.669×10^{-25}
2062.158	2.87×10^{-22}	3.812×10^{-25}

$$\text{Total } \sigma_{2O_3} = 1.37 \times 10^{-21} \text{ cm}^2$$

Appendix H

CO₂ Extinction Coefficient ("Off"-Resonance)

<u>h(km)</u>	<u>$\sigma_{\text{CO}_2} (\text{cm}^2)$</u>	<u>$N_{\text{CO}_2} (\text{cm}^{-3})$</u>	<u>$N_{\text{CO}_2} \sigma_{\text{CO}_2} \times 10^5 (\text{km}^{-1})$</u>
0	1.361×10^{-21}	8.405×10^{15}	1.144
1	7.200×10^{-22}	7.626×10^{15}	.605
2	4.94×10^{-22}	6.907×10^{15}	.377
3	3.33×10^{-22}	6.240×10^{15}	.230
4	2.21×10^{-22}	5.623×10^{15}	.124
5	1.43×10^{-22}	5.052×10^{15}	7.22×10^{-2}
6	9.15×10^{-23}	4.531×10^{15}	4.15×10^{-2}
7	5.71×10^{-23}	4.049×10^{15}	2.31×10^{-2}
8	3.47×10^{-23}	3.607×10^{15}	1.25×10^{-2}
9	2.06×10^{-23}	3.205×10^{15}	6.60×10^{-3}
10	1.20×10^{-23}	2.837×10^{15}	3.40×10^{-3}
11	6.65×10^{-24}	2.503×10^{15}	1.66×10^{-3}
12	5.64×10^{-24}	2.140×10^{15}	1.21×10^{-3}
13	4.85×10^{-24}	1.829×10^{15}	8.87×10^{-4}
14	4.14×10^{-24}	1.564×10^{15}	6.47×10^{-4}
15	3.55×10^{-24}	1.336×10^{15}	4.74×10^{-4}
16	3.01×10^{-24}	1.142×10^{14}	3.44×10^{-4}
17	2.58×10^{-24}	9.765×10^{14}	2.52×10^{-4}
18	2.21×10^{-24}	8.346×10^{14}	1.84×10^{-4}
19	1.89×10^{-24}	7.135×10^{14}	1.35×10^{-4}
20	1.61×10^{-24}	6.102×10^{14}	9.82×10^{-5}

21	1.47×10^{-24}	5.194×10^{14}	7.64×10^{-5}
22	1.35×10^{-24}	4.425×10^{14}	5.97×10^{-5}
23	1.23×10^{-24}	3.775×10^{14}	6.46×10^{-5}
24	1.13×10^{-24}	3.221×10^{14}	3.64×10^{-5}
25	1.03×10^{-24}	2.751×10^{14}	2.83×10^{-5}
26	9.39×10^{-25}	2.351×10^{14}	2.21×10^{-5}
27	8.61×10^{-25}	2.010×10^{14}	1.73×10^{-5}
28	7.90×10^{-25}	1.721×10^{14}	1.36×10^{-5}
29	7.19×10^{-25}	1.474×10^{14}	1.06×10^{-5}
30	6.59×10^{-25}	1.263×10^{14}	8.32×10^{-6}

Appendix I

CO Extinction Coefficient ("Off"-Resonance)					
<u>h(km)</u>	<u>T(°K)</u>	<u>N_{CO}(cm⁻³)</u>	<u>P/P_S</u>	<u>σ_{2CO}(cm⁻²)</u>	<u>σ_{2CO}N_{CO}×10⁵(km⁻¹)</u>
0	296	1.884×10 ¹²	1.0	3.585×10 ⁻²²	6.75×10 ⁻⁵
1	281.7	1.710×10 ¹²	.887	2.189×10 ⁻²²	3.74×10 ⁻⁵
2	275.2	1.549×10 ¹²	.785	1.613×10 ⁻²²	2.50×10 ⁻⁵
3	286.7	1.399×10 ¹²	.692	1.064×10 ⁻²²	1.49×10 ⁻⁵
4	262.2	1.261×10 ¹²	.609	8.410×10 ⁻²³	1.06×10 ⁻⁵
5	255.7	1.133×10 ¹²	.533	5.928×10 ⁻²³	6.72×10 ⁻⁶
6	249.2	1.016×10 ¹²	.466	4.132×10 ⁻²³	4.20×10 ⁻⁶
7	242.7	9.078×10 ¹¹	.406	2.841×10 ⁻²³	2.57×10 ⁻⁶
8	236.2	8.087×10 ¹¹	.352	1.904×10 ⁻²³	1.54×10 ⁻⁶
9	229.7	7.186×10 ¹¹	.304	1.255×10 ⁻²³	9.02×10 ⁻⁷
10	223.3	6.362×10 ¹¹	.262	8.159×10 ⁻²⁴	5.19×10 ⁻⁷
11	216.8	5.612×10 ¹¹	.224	5.124×10 ⁻²⁴	2.88×10 ⁻⁷
12	216.7	4.799×10 ¹¹	.191	4.355×10 ⁻²⁴	2.09×10 ⁻⁷
13	216.7	4.101×10 ¹¹	.164	3.744×10 ⁻²⁴	1.54×10 ⁻⁷
14	216.7	3.506×10 ¹¹	.140	3.196×10 ⁻²⁴	1.12×10 ⁻⁷
15	216.7	2.996×10 ¹¹	.120	2.739×10 ⁻²⁴	8.21×10 ⁻⁸
16	216.7	2.561×10 ¹¹	.102	2.328×10 ⁻²⁴	5.96×10 ⁻⁸
17	216.7	2.189×10 ¹¹	.0873	1.994×10 ⁻²⁴	4.36×10 ⁻⁸
18	216.7	1.871×10 ¹¹	.0747	1.706×10 ⁻²⁴	3.19×10 ⁻⁸
19	216.7	1.600×10 ¹¹	.0638	1.457×10 ⁻²⁴	2.33×10 ⁻⁸
20	216.7	1.368×10 ¹¹	.0546	1.246×10 ⁻²⁴	1.71×10 ⁻⁸

21	217.6	1.165×10^{11}	.0467	1.110×10^{-24}	1.29×10^{-8}
22	218.6	9.922×10^{10}	.0399	9.945×10^{-25}	9.87×10^{-9}
23	219.6	8.464×10^{10}	.0342	8.980×10^{-25}	7.60×10^{-9}
24	220.6	7.221×10^{10}	.0293	8.039×10^{-25}	5.80×10^{-9}
25	220.6	6.167×10^{10}	.0293	7.262×10^{-25}	4.48×10^{-9}
26	222.5	5.270×10^{10}	.0216	6.454×10^{-25}	3.40×10^{-9}
27	223.5	4.507×10^{10}	.0186	5.837×10^{-25}	2.63×10^{-9}
28	224.5	3.858×10^{10}	.0160	5.262×10^{-25}	2.03×10^{-9}
29	225.5	3.304×10^{10}	.0137	4.715×10^{-25}	1.56×10^{-9}
30	226.5	2.832×10^{10}	.0118	4.230×10^{-25}	1.20×10^{-9}

Appendix J

<u>O₃ Extinction Coefficient ("Off"-Resonance)</u>			
<u>h(km)</u>	<u>σ_{2O₃} (cm²)</u>	<u>N_{O₃} (cm⁻³)</u>	<u>N_{O₃} σ_{2O₃} x 10⁵ (km⁻¹)</u>
0	1.37 x 10 ⁻²¹	6.8 x 10 ¹¹	9.32 x 10 ⁻⁵
2	9.30 x 10 ⁻²²	6.8 x 10 ¹¹	6.32 x 10 ⁻⁵
4	6.44 x 10 ⁻²²	5.8 x 10 ¹¹	3.74 x 10 ⁻⁵
6	4.33 x 10 ⁻²²	5.7 x 10 ¹¹	2.47 x 10 ⁻⁵
8	2.81 x 10 ⁻²²	6.5 x 10 ¹¹	1.83 x 10 ⁻⁵
10	1.76 x 10 ⁻²²	1.13 x 10 ¹²	1.99 x 10 ⁻⁵
12	1.16 x 10 ⁻²²	2.02 x 10 ¹²	2.35 x 10 ⁻⁵
14	8.48 x 10 ⁻²³	2.35 x 10 ¹²	2.00 x 10 ⁻⁵
16	6.18 x 10 ⁻²³	2.95 x 10 ¹²	1.83 x 10 ⁻⁵
18	4.53 x 10 ⁻²³	4.04 x 10 ¹²	1.83 x 10 ⁻⁵
20	3.31 x 10 ⁻²³	4.77 x 10 ¹²	1.58 x 10 ⁻⁵
22	2.50 x 10 ⁻²³	4.86 x 10 ¹²	1.22 x 10 ⁻⁵
24	1.89 x 10 ⁻²³	4.54 x 10 ¹²	8.60 x 10 ⁻⁶
26	1.43 x 10 ⁻²³	4.03 x 10 ¹²	5.75 x 10 ⁻⁶
28	1.09 x 10 ⁻²³	3.24 x 10 ¹²	5.53 x 10 ⁻⁶
30	8.29 x 10 ⁻²⁴	2.52 x 10 ¹²	2.09 x 10 ⁻⁶
1			7.65 x 10 ⁻⁵
3			4.83 x 10 ⁻⁵
5			3.01 x 10 ⁻⁵
7			2.11 x 10 ⁻⁵
9			1.84 x 10 ⁻⁵

Appendix K

H₂O Extinction Coefficient ("Off"-Resonance)

<u>h(km)</u>	<u>$\sigma_{\text{H}_2\text{O}}(\text{cm}^2)$</u>	<u>$N_{\text{H}_2\text{O}}(\text{cm}^{-3})$</u>	<u>$N_{\text{H}_2\text{O}} \sigma_{\text{H}_2\text{O}} \times 10^5 (\text{km}^{-1})$</u>
0	9.38×10^{-25}	1.910×10^{17}	1.881×10^{-2}
1	6.33×10^{-25}	1.368×10^{17}	8.660×10^{-3}
2	4.77×10^{-25}	9.520×10^{16}	4.541×10^{-3}
4	2.62×10^{-25}	3.456×10^{16}	9.054×10^{-4}
6	1.36×10^{-25}	1.217×10^{16}	1.655×10^{-4}
8	6.64×10^{-25}	3.778×10^{15}	2.509×10^{-5}
10	3.03×10^{-26}	5.941×10^{14}	1.800×10^{-6}
12	1.68×10^{-26}	1.173×10^{14}	1.970×10^{-7}
14	1.23×10^{-26}	2.501×10^{13}	3.077×10^{-8}
16	8.95×10^{-27}	1.827×10^{13}	1.636×10^{-9}
18	6.56×10^{-27}	1.335×10^{13}	8.760×10^{-9}
20	4.79×10^{-27}	1.331×10^{13}	6.336×10^{-9}
22	3.80×10^{-27}	1.545×10^{13}	5.872×10^{-9}
24	3.03×10^{-27}	1.811×10^{13}	5.488×10^{-9}
26	2.42×10^{-27}	2.120×10^{13}	5.130×10^{-9}
28	1.94×10^{-27}	1.518×10^{13}	2.946×10^{-9}
30	1.55×10^{-27}	1.078×10^{13}	1.703×10^{-9}
3			2.030×10^{-3}
5			3.85×10^{-4}
7			6.30×10^{-5}
9			6.66×10^{-6}

Appendix L

Hot CO₂ Absorption Cross Section ("Off-Resonance")

	<u>h(km)</u>	<u>P/P_s</u>	<u>(T_s/T)^{3/2}</u>	<u>$\frac{Q_v(T_2)}{Q_v(T)}$</u>	<u>$\sigma_{2CO_2}^H$ (cm²)</u>
<u>T=400 K</u>					
	0	1	.637	.889	1.699 x 10 ⁻²⁰
	1	.887	.637	.889	1.507 x 10 ⁻²⁰
	2	.785	.637	.889	1.334 x 10 ⁻²⁰
<u>T=500 K</u>					
	0	1	.456	.772	6.145 x 10 ⁻²⁰
	1	.887	.465	.772	5.451 x 10 ⁻²⁰
	2	.785	.456	.772	4.824 x 10 ⁻²⁰
<u>T=600 K</u>					
	0	1	.347	.661	1.295 x 10 ⁻¹⁹
	1	.887	.347	.661	1.149 x 10 ⁻¹⁹
	2	.785	.347	.661	1.017 x 10 ⁻¹⁹
<u>T=700 K</u>					
	0	1	.275	.361	2.015 x 10 ⁻¹⁹
	1	.887	.275	.361	1.787 x 10 ⁻¹⁹
	2	.785	.275	.361	1.581 x 10 ⁻¹⁹
<u>T=800 K</u>					
	0	1	.225	.475	2.617 x 10 ⁻¹⁹
	1	.887	.225	.475	2.322 x 10 ⁻¹⁹
	2	.785	.225	.475	2.055 x 10 ⁻¹⁹

T=900 K

0	1	.189	.402	3.035×10^{-19}
1	.887	.189	.402	2.692×10^{-19}
2	.785	.189	.402	2.382×10^{-19}

T=1000 K

0	1	.161	.341	3.243×10^{-19}
1	.887	.161	.341	2.876×10^{-19}
2	.785	.161	.341	2.546×10^{-19}

Vita

Robert Harold Wank was born on 26 June 1950 in St. Johns, Michigan. He graduated from high school in Muskegon, Michigan in 1968 and attended USMA, West Point, New York, from which he received the degree of Bachelor of Science in Engineering in June 1972. Upon graduation he was commissioned in the Corps of Engineers, and attended the Engineer Officer Basic Course at Fort Belvoir, Virginia, and Airborne School at Fort Benning, Georgia. After serving as a combat engineer platoon leader and executive officer at Fort Richardson, Alaska for 39 months, he returned to Fort Belvoir to complete the Engineer Officer Advanced Course. He then served 2½ years as a combat engineer company commander and staff officer at Fort Ord, California, followed by 2 years as an area commander in the U.S. Army Recruiting Command in St. Louis, Missouri. He entered the School of Engineering, Air Force Institute of Technology, in June 1981.

Permanent Address: 3512 Osceola Dr.
Muskegon, MI 49441

UNCLASSIFIED

SECURITY CLASSIFICATION OF THIS PAGE (When Data Entered)

REPORT DOCUMENTATION PAGE		READ INSTRUCTIONS BEFORE COMPLETING FORM
1. REPORT NUMBER AFIT/GEP/PH/82D-25	2. GOVT ACCESSION NO. AD-A164 308	3. RECIPIENT'S CATALOG NUMBER
4. TITLE (and Subtitle) DETECTION OF ATMOSPHERIC CARBON DIOXIDE FROM A SHUTTLE-BORNE LIDAR		5. TYPE OF REPORT & PERIOD COVERED MS Thesis
		6. PERFORMING ORG. REPORT NUMBER
7. AUTHOR(s) Robert H. Wank Captain, USA		8. CONTRACT OR GRANT NUMBER(s)
9. PERFORMING ORGANIZATION NAME AND ADDRESS Air Force Institute of Technology (AFIT-EN) Wright-Patterson AFB, Ohio 45435		10. PROGRAM ELEMENT, PROJECT, TASK AREA & WORK UNIT NUMBERS
11. CONTROLLING OFFICE NAME AND ADDRESS		12. REPORT DATE December 1982
		13. NUMBER OF PAGES 134
14. MONITORING AGENCY NAME & ADDRESS (if different from Controlling Office)		15. SECURITY CLASS. (of this report) UNCLASSIFIED
		15a. DECLASSIFICATION/DOWNGRADING SCHEDULE
16. DISTRIBUTION STATEMENT (of this Report) Approved for public release; distribution unlimited		
17. DISTRIBUTION STATEMENT (of the abstract entered in Block 20, if different from Report)		
18. SUPPLEMENTARY NOTES Approved for Public Release, IAW AFR 190-1 <i>LYNN E. WOLAVEN</i> 16 JAN 83 Dean for Research and Professional Development Air Force Institute of Technology (AFIT) Wright-Patterson AFB OH 45423		
19. KEY WORDS (Continue on reverse side if necessary and identify by block number) Differential Absorption Lidar DIAL Atmospheric Carbon Dioxide Shuttleborne Lidar		
20. ABSTRACT (Continue on reverse side if necessary and identify by block number) See reverse side		

DD FORM 1 JAN 73 1473

EDITION OF 1 NOV 65 IS OBSOLETE

UNCLASSIFIED

SECURITY CLASSIFICATION OF THIS PAGE (When Data Entered)

UNCLASSIFIED

SECURITY CLASSIFICATION OF THIS PAGE(When Data Entered)

Remote sensing of atmospheric carbon dioxide from a shuttle-borne differential absorption lidar (DIAL) was investigated. The investigation followed the basic frequency recommendations of Korb, which included "on"-resonance frequency at the P(34) line of the (11'0-03'0), absorption band of CO₂. Extinction coefficients for CO₂, H₂O, CO, O₃, Rayleigh, and Mie scattering were determined to compute estimated return signal strengths from various altitudes. Direct detection was found to be unsuitable, but heterodyne detection provided adequate signal-to-noise ratios. Cross sections for hot CO₂ were also calculated, and maximum detectable CO₂ concentrations were determined. Finally, an error analysis of predicted CO₂ concentrations was made, which determined that due to the large CO₂ "on"-resonance extinction coefficient, accurate measurements of CO₂ below five kilometers could not be made.

*Korb, C.L. et. al. "A Lidar Technique for Measurement of Atmospheric Carbon Dioxide," Proceedings of the Tenth International Laser Radar Conference. 105-106. Silver Springs, Maryland: Committee on Laser Atmospheric Studies, October 1980.

UNCLASSIFIED

SECURITY CLASSIFICATION OF THIS PAGE(When Data Entered)

END

FILMED

4-81

DTIC